The Canadian Mineralogist
Vol. 38, pp. 975-994 (2000)

OCCURRENCE, ALTERATION PATTERNS AND COMPOSITIONAL VARIATION OF PEROVSKITE IN KIMBERLITES

ANTON R. CHAKHMOURADIAN[§] AND ROGER H. MITCHELL

Department of Geology, Lakehead University, 955 Oliver Road, Thunder Bay, Ontario P7B 5E1, Canada

ABSTRACT

The present work summarizes a detailed investigation of perovskite from a representative collection of kimberlites, including samples from over forty localities worldwide. The most common modes of occurrence of perovskite in archetypal kimberlites are discrete crystals set in a serpentine–calcite mesostasis, and reaction-induced rims on earlier-crystallized oxide minerals (typically ferroan geikielite or magnesian ilmenite). Perovskite precipitates later than macrocrystal spinel (aluminous magnesian chromite), and nearly simultaneously with "reaction" Fe-rich spinel (*sensu stricto*), and groundmass spinels belonging to the magnesian ulvöspinel – magnetite series. In most cases, perovskite crystallization ceases prior to the resorption of groundmass spinels and formation of the atoll rim. During the final evolutionary stages, perovskite commonly becomes unstable and reacts with a CO_2-rich fluid. Alteration of perovskite in kimberlites involves resorption, cation leaching and replacement by late-stage minerals, typically TiO_2, ilmenite, titanite and calcite. Replacement reactions are believed to take place at temperatures below 350°C, $P < 2$ kbar, and over a wide range of $a(Mg^{2+})$ values. Perovskite from kimberlites approaches the ideal formula $CaTiO_3$, and normally contains less than 7 mol.% of other end-members, primarily lueshite ($NaNbO_3$), loparite ($Na_{0.5}Ce_{0.5}TiO_3$), and $CeFeO_3$. Evolutionary trends exhibited by perovskite from most localities are relatively insignificant and typically involve a decrease in *REE* and Th contents toward the rim (normal pattern of zonation). A reversed pattern is much less common, and probably results from re-equilibration of perovskite with a kimberlitic magma modified by assimilation or contamination processes. Oscillatory zonation on a fine scale is comparatively uncommon, and involves subtle variations in *LREE*, Th, Nb and Fe. Relatively high levels of *LREE*, Th and Nb observed in perovskite from some occurrences (Lac de Gras and Kirkland Lake in Canada, Obnazhennaya in Yakutia) probably result from inherent enrichment of the host kimberlites in "incompatible" elements. In some cases (Benfontein in South Africa), differentiation processes may have contributed to the accumulation of "incompatible" elements in perovskite.

Keywords: perovskite, alteration, textures, kimberlite.

SOMMAIRE

Nous présentons ici les résultats d'une étude approfondie de la pérovskite telle qu'elle se présente dans une collection représentative de kimberlites, les échantillons ayant été prélevés à 40 endroits. Dans les kimberlites types, la pérovskite se présente en cristaux distincts dans une pâte composée de serpentine et de calcite, ou bien en liseré réactionnel sur des oxydes précoces (en général, geikielite ferreuse ou ilménite magnésienne). La pérovskite cristallise après le spinelle qui se présente sous forme de macrocrystal (chromite alumineuse magnésienne), et à peu près en même temps que le spinelle *sensu stricto* riche en fer d'origine réactionnelle et le spinelle de la pâte, faisant partie de la série ulvöspinelle magnésien – magnétite. Dans la plupart des cas, la cristallisation de la pérovskite a cessé avant que ne commence la résorption du spinelle de la pâte et la formation d'une bordure en atoll. Au cours des stades ultimes d'évolution, il est courant pour la pérovskite de montrer des signes d'instabilité et d'une réaction avec une phase fluide riche en CO_2. Dans les kimberlites, l'altération de la pérovskite se déroule par résorption, lessivage des cations, et remplacement par des minéraux tardifs, par exemple TiO_2, ilménite, titanite et calcite. Les réactions de remplacement auraient lieu à une température inférieure à 350°C, $P < 2$ kbar, et sur un large intervalle de valeurs de $a(Mg^{2+})$. La pérovskite des kimberlites se rapproche de la formule idéale $CaTiO_3$, et contient normalement moins de 7% (proportion molaire) des autres pôles, surtout lueshite ($NaNbO_3$), loparite ($Na_{0.5}Ce_{0.5}TiO_3$), et $CeFeO_3$. La variabilité en composition de la pérovskite à la plupart des sites échantillonnés est relativement restreinte et implique typiquement une diminution de la teneur en terres rares et en thorium vers la bordure (zonation dite normale). Les exemples de zonation inverse sont beaucoup moins répandus, et résulteraient d'un ré-équilibrage de la pérovskite avec un magma kimberlitique modifié par assimilation ou contamination. Une zonation oscillatoire sur une fine échelle est relativement rare, et implique des variations subtiles en concentrations des terres rares légères, Th, Nb et Fe. Les teneurs relativement élevées de la pérovskite en terres rares, Th et Nb à certains endroits (Lac de Gras et Kirkland Lake au Canada, Obnazhennaya en Yakoutie) résulteraient du degré intrinsèque d'enrichissement de l'hôte kimberlitique en éléments "incompatibles". Dans certains cas, par exemple Benfontein en Afrique du Sud, les processus de différenciation pourraient aussi avoir contribué à l'accumulation des éléments "incompatibles" dans la pérovskite.

(Traduit par la Rédaction)

Mots-clés: pérovskite, altération, textures, kimberlite.

[§] *E-mail address*: achakhmo@gale.lakeheadu.ca

INTRODUCTION

Perovskite is a characteristic minor constituent of archetypal kimberlites, and is typically present in concentrations below 10 vol.% (Mitchell 1986). The abundance of this mineral is higher in differentiated hypabyssal-facies kimberlites such as the Benfontein sill in South Africa (Dawson & Hawthorne 1973). Numerous publications on the petrography and mineralogy of kimberlites contain descriptions of perovskite. Many of these descriptions provide basic compositional data on perovskite, but typically lack information on minor, but important components such as rare-earth elements (*REE*), Nb and Th. Although the majority of perovskite from kimberlite is stoichiometrically close to the end-member composition $CaTiO_3$, some occurrences do contain perovskite with elevated levels of incompatible elements (*e.g.*, Green Mountain in Colorado: Boctor & Meyer 1979). Clearly, variations in perovskite composition arise from different patterns of evolution of the host kimberite. However, the available analytical and paragenetic data commonly are insufficient to ascribe these compositional variations to inherent anomalous enrichment of some kimberlitic magmas in incompatible elements, assimilation of crustal material or other processes that could enhance concentrations of light *REE*, Nb and Th in the system. The pattern of alteration typically exhibited by perovskite is another aspect that could provide some important clues to the evolution of kimberlites, but has been largely neglected in the previous studies. Mitchell & Chakhmouradian (1998a) also demonstrated that perovskite instability in kimberlites has direct implications for the problem of long-term conservation of nuclear wastes.

Here, we summarize results of the detailed investigation of perovskite from a representative collection of kimberlites that includes samples from over forty kimberlite intrusions from twenty-one occurrences worldwide. Data on individual intrusions, fields and provinces, as well as detailed petrographic descriptions of representative rock samples from most occurrences, can be found in Mitchell (1986, 1997a).

OCCURRENCE

The formation of kimberlite is a complex, multistage process involving upper-mantle metasomatism, partial melting, assimilation and contamination with mantle and crustal material, primary magmatic crystallization, re-equilibration, low- to medium-temperature hydrothermal events, and subsolidus alteration. The complex history of crystallization results in diverse parageneses in which perovskite (*sensu lato*) occurs in kimberlites. These parageneses include:

(i) The fine-grained primary matrix or groundmass of the rock, where perovskite is associated with olivine, spinel, apatite, calcite, serpentine, monticellite, ilmenite and sulfides (Mitchell 1986);

(ii) reaction-induced rims on earlier-crystallized Ti-bearing, primarily oxide minerals (Smirnov 1959, Boctor & Boyd 1980, 1981);

(iii) relict fragments in complex multiphase pseudomorphs typically consisting of Ti-oxide phases and calcite (Mitchell & Chakhmouradian 1998a);

(iv) xenoliths of upper-mantle rocks, in association with niobian titanite, magnesian ilmenite, spinel and Nb–Cr-enriched rutile (Haggerty 1987);

(v) inclusions in diamond (Kopylova *et al.* 1997a, b).

The first three parageneses are, by far, the most common modes of perovskite occurrence in kimberlite. Perovskite of type (ii) has been also described as a composite inclusion in diamond, and interpreted as "epigenetic", *i.e.*, derived from a fluid percolating through the diamond host (Kopylova *et al.* 1997a). Some perovskite-group minerals found as inclusions in diamonds and mantle xenoliths are very unusual in terms of composition, being enriched in Nb (3.5–28.0 wt.% Nb_2O_5), Cr (1.0–7.8 wt.% Cr_2O_3), and alkalis (1.5–4.6 wt.% $Na_2O + K_2O$) (Haggerty 1987, Kopylova *et al.* 1997b). High concentrations of Nb and Cr also characterize some other minerals found as xenocrysts in kimberlites (*e.g.*, rutile), but are generally atypical of perovskite from parageneses (i)–(iii). Nb–Cr-rich perovskite-group phases are rare in kimberlites, and, thus far, have been described only from Jagersfontein in South Africa, and River Ranch in Zimbabwe (Haggerty 1987, Kopylova *et al.* 1997b). The scarcity of these minerals may indicate their limited stability under the upper-mantle conditions, especially relative to other oxide phases accommodating "incompatible" elements (*e.g.*, ilmenite, armalcolite, lindsleyite and hawthorneite). As crystallization of Nb–Cr-rich perovskite in parageneses (iv) and (v) is clearly related to the processes of metasomatism in the upper mantle, rather than evolution of a kimberlitic magma, below we consider only perovskite (*sensu stricto*) found in parageneses (i)–(iii).

In most kimberlite occurrences, perovskite crystallizes as euhedral or subhedral, rounded crystals set in a mesostasis consisting of calcite and serpentine. Typically, in hypabyssal-facies rocks, crystals of perovskite are randomly disseminated throughout the groundmass (Figs. 1A, B). Less common are euhedral inclusions of perovskite in groundmass micas of phlogopite or phlogopite–kinoshitalite composition (Fig. 1C). In some kimberlite sills, *e.g.*, at Benfontein and Wesselton (South Africa), perovskite and spinel (with or without olivine and phlogopite) form cumulus textures arising from magmatic sedimentation phenomena (Dawson & Hawthorne 1973, Mitchell 1984). A characteristic textural feature of such cumulate layers consists of microdiapirs of calcite resulting from mobilization of intercumulus carbonate-rich material from an underlying horizon (Fig. 1D). Also common in kimberlites are "necklaces" of perovskite crystals around earlier-formed macrocrysts or phenocrysts of olivine (Figs. 1E, F). In diatreme-facies rocks, perovskite is predominantly concentrated in pelletal lapilli (Fig. 1G), and in crater-facies rocks in similar juvenile lapilli. Individual crystals of perovskite may be cubic or cubo-octahedral in habit (Wesselton mine), and only rarely compose interpenetration twins of the "fluorite type" (Benfontein). Kimberlites of the Kuonamskii and Chuktukonskii fields in Yakutia were reported to contain skeletal crystals of diverse morphology (Blagul'kina & Tarnovskaya 1975). The size of perovskite crystals in a kimberlite groundmass varies from less than 1 μm to nearly 0.5 mm (Fort à la Corne, Saskatchewan: Fig. 1F). At Kirkland Lake (Ontario), a macrocrystic kimberlite is unusual in containing both small discrete crystals and glomerocrysts of perovskite up to 0.8 mm across. In most occurrences, however, crystals are relatively uniform in size, and typically range from 20 to 50 μm across.

Perovskite is a characteristic product of reaction between early Ti-bearing phases and the kimberlitic magma. In most cases, precursor minerals are Ti-bearing oxides belonging to the macrocryst suite. Among these, the ilmenite-group minerals, *i.e.*, Cr–Fe^{3+}-enriched and Mn-poor magnesian ilmenite and ferroan geikielite are the most common precursor phases (Figs. 1H, I). The thickness of a reaction-induced rim of perovskite on ilmenite ranges from a few μm to 60 μm. In some kimberlites, *e.g.*, at Lac de Gras field (NWT) and Kirkland Lake, the formation of the perovskite rim was preceded by crystallization of Mg–Ti-rich and Cr-poor magnesian ulvöspinel – ulvöspinel – magnetite (or MUM) spinel (Fig. 1J). There are also more complex intergrowths of MUM spinels with perovskite, in which primary macrocrystic ilmenite is preserved only as small fragments (Fig. 1K). Mantling of other macrocrystic oxide phases (*e.g.*, chromian spinel) by perovskite is much less common (Mitchell 1986, and references therein). During the present study, we also observed a reaction-induced rim of perovskite on priderite, a rare K–(Fe,Mg) titanate atypical of kimberlites (Fig. 1L). Perovskite also has been described as a component of reaction-induced mantles on macrocrystic garnet (for instance, from the Mir diatreme in Yakutia: Vishnevskii *et al.* 1984). In the Mir kimberlite, perovskite in an assemblage with MUM-type spinel and phlogopite comprises corona-textured kelyphytic rims on Cr-depleted and Ti-enriched pyrope (Vishnevskii *et al.* 1984).

In the majority of kimberlites, perovskite crystallized later than macrocrystic spinel (aluminous magnesiochromite or magnesian chromite), and nearly simultaneously with groundmass MUM spinels (Fig. 2A). Typically, the crystallization of perovskite ceases prior to the resorption of MUM spinels and development of an atoll rim (Fig. 2B). In rare cases, however, atoll spinels are fully enclosed by perovskite, indicating that the precipitation of the latter mineral proceeded through the resorption stage (Fig. 2C). In "contaminated" varieties of kimberlite, perovskite crystallizes nearly contemporaneously with ferroan spinel, but prior to the formation of the atoll rim (Figs. 2D, E). Note that atoll textures undoubtedly have a multiplicity of origins, and are known to form after both MUM-type spinel and ferroan spinel (Mitchell 1986). Resorption of the early generations of spinel and crystallization of a magnetite-rich rim may result from a rapid decrease in temperature along the QFM buffer (Mitchell & Clarke 1976) or increase in $f(O_2)$ (Pasteris 1983) during the terminal stages of precipitation of the groundmass. In addition to magnesian chromite and MUM spinels, perovskite may also enclose euhedral crystals of macrocrystic phlogopite and ilmenite (Fig. 2F).

ALTERATION

Perovskite is unstable in a CO_2-rich, weakly acidic environment (Mitchell & Chakhmouradian 1998a). During the final stages of kimberlite evolution, this mineral commonly undergoes cation leaching and replacement by other Ti-bearing minerals. A titanium dioxide (TiO_2) phase is, by far, the most common product of perovskite alteration in kimberlites. Definitive identification of this phase is normally precluded by very small size, and its intimate association with other products of replacement (see below). In most studies, titanium dioxide mantling perovskite in kimberlites has been provisionally identified as rutile, the most stable TiO_2 polymorph. However, Mitchell & Chakhmouradian (1998a) have shown that, at least in some occurrences (*e.g.*, Iron Mountain, Wyoming), the product of perovskite alteration is anatase, rather than rutile. Unfortunately, there are very few studies of perovskite instability in other rock types. It has been demonstrated that in carbonatites and laterites, perovskite is typically converted to anatase (Kapustin 1964, Banfield & Veblen 1992, Mitchell & Chakhmouradian 1998a). Banfield & Veblen (1992) also observed the *B*-modification of TiO_2 in an assemblage with secondary anatase in laterites. Notably, neither rutile nor brookite has been *conclusively* proven to replace perovskite in the natural environment. As the stability of rutile, anatase and brookite is controlled not only by thermodynamic factors, but also by concentration of minor elements in their composition (Grunin *et al.* 1983), different kimberlites may contain different polymorphs of TiO_2 in the replacement assemblage. Consequently, we refer to these minerals simply as TiO_2, unless the exact identification has been made using optical microscopy.

Formation of TiO_2 at the expense of $CaTiO_3$ involves leaching of Ca from the perovskite structure and its subsequent deposition in the form of calcite (Nesbitt *et al.* 1981):

$$CaTiO_3 + CO_2 = TiO_2 + CaCO_3 \tag{1}$$

Calcite is normally deposited in the immediate vicinity of perovskite, giving the TiO_2 rim a cavernous or "spongy" appearance (Fig. 3A). In some cases, a TiO_2 rim is separated from a relict perovskite core by an

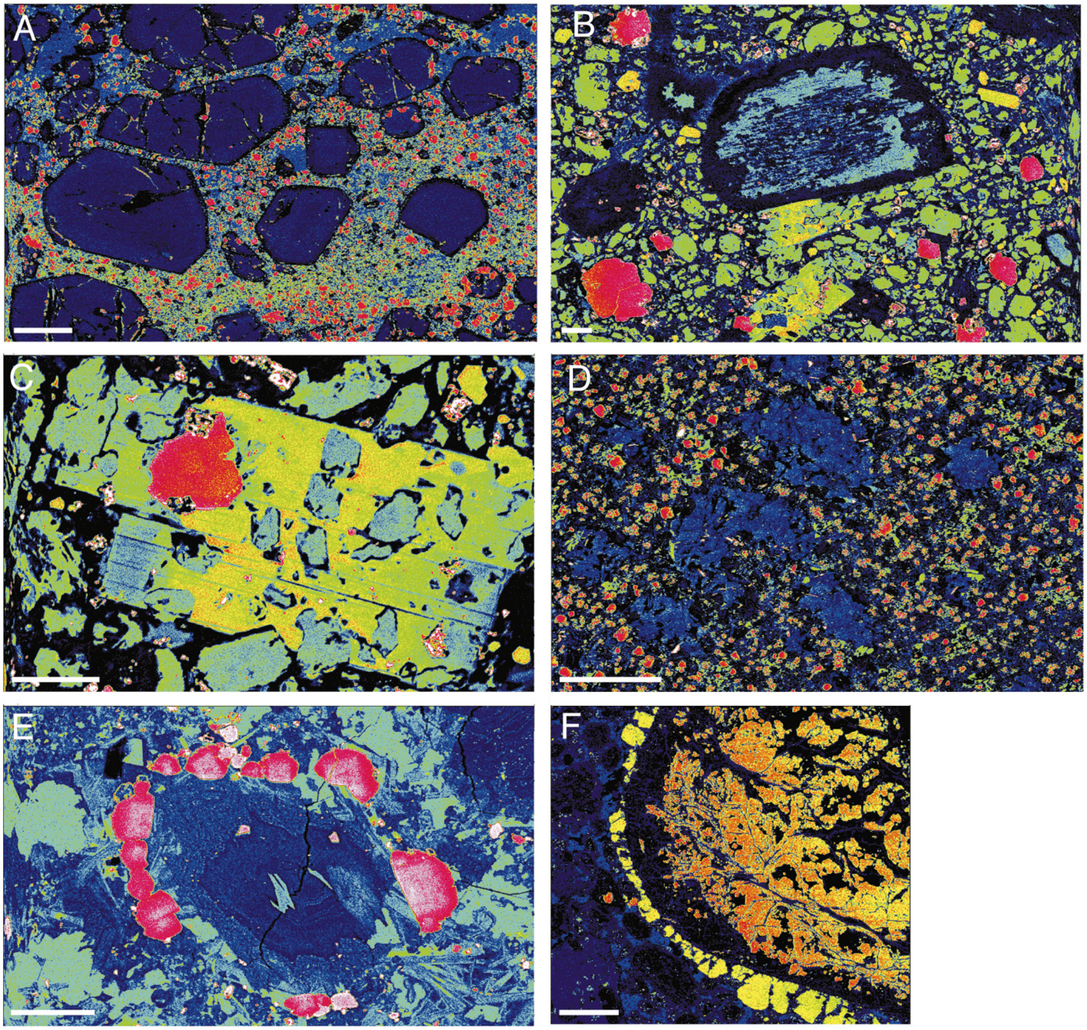

FIG. 1. False-color back-scattered electron (BSE) images of some characteristic modes of occurrence of perovskite in kimberlites. The images in this figure, and in Figures 2–4, were acquired with the LINK–ISIS AUTOBEAM software using a Hitachi 570 scanning electron microscope. The images were given false colors using the LINK–ISIS SPEEDMAP software package, and stored as "pcx" files. Scale bar is 450 μm for the images (A,D,F,G), 50 μm for (B,C,E and H) and 10 μm for (I–L). (A) Randomly distributed discrete crystals of perovskite and spinel (red), and olivine macrocrysts (dark blue) in a calcite – serpentine matrix (blue); note enrichment of the lower part of the image in apatite (green). Benfontein mine, South Africa. (B) Euhedral crystals of perovskite (red), spinel (red, smaller), monticellite (green) and apatite (yellow) in a calcite – serpentine matrix. The large blue grain is serpentinized olivine partly replaced by calcite (pale blue); yellowish green laths are groundmass phlogopite. Elwin Bay, Nunavut. (C) Euhedral inclusions of perovskite (red), monticellite (greenish blue) and spinel (red to white) in groundmass phlogopite. Elwin Bay, Nunavut. (D) Cumulate layer of perovskite, spinel (red) and phlogopite (greenish) protruded by micro-diapirs of calcite (blue). Wesselton Sill, South Africa. (E) "Necklace"-textured arrangement of perovskite (red) around serpentinized olivine (blue). Note that perovskite crystals are weakly zoned, with a core enriched in *REE*, Th, Na and Nb. Matsoku, Lesotho. (F) "Necklace" of large crystals of perovskite (yellow) around an "iddingsitized" olivine macrocryst (orange). Fort à la Corne, Saskatchewan. (G) Globular segregation containing perovskite, spinel (red) and olivine macrocrysts (blue). Chomur, Yakutia. (H) Reaction-induced rim of perovskite (green) on a zoned macrocryst of magnesian ilmenite – ferroan geikielite (green to bluish green) set in a matrix of calcite and serpentine (black). Premier mine, South Africa. (I) Perovskite (green) developed as a reaction-induced rim terminated with euhedral crystals, on a macrocryst of geikielite (blue). Fort à la Corne, Saskatchewan. (J) Macrocryst of magnesian ilmenite (blue) successively rimmed by MUM spinel (green) and *REE*–Fe- rich perovskite (red). Lac de Gras, NWT. (K) Magnesian ilmenite with exsolution textures

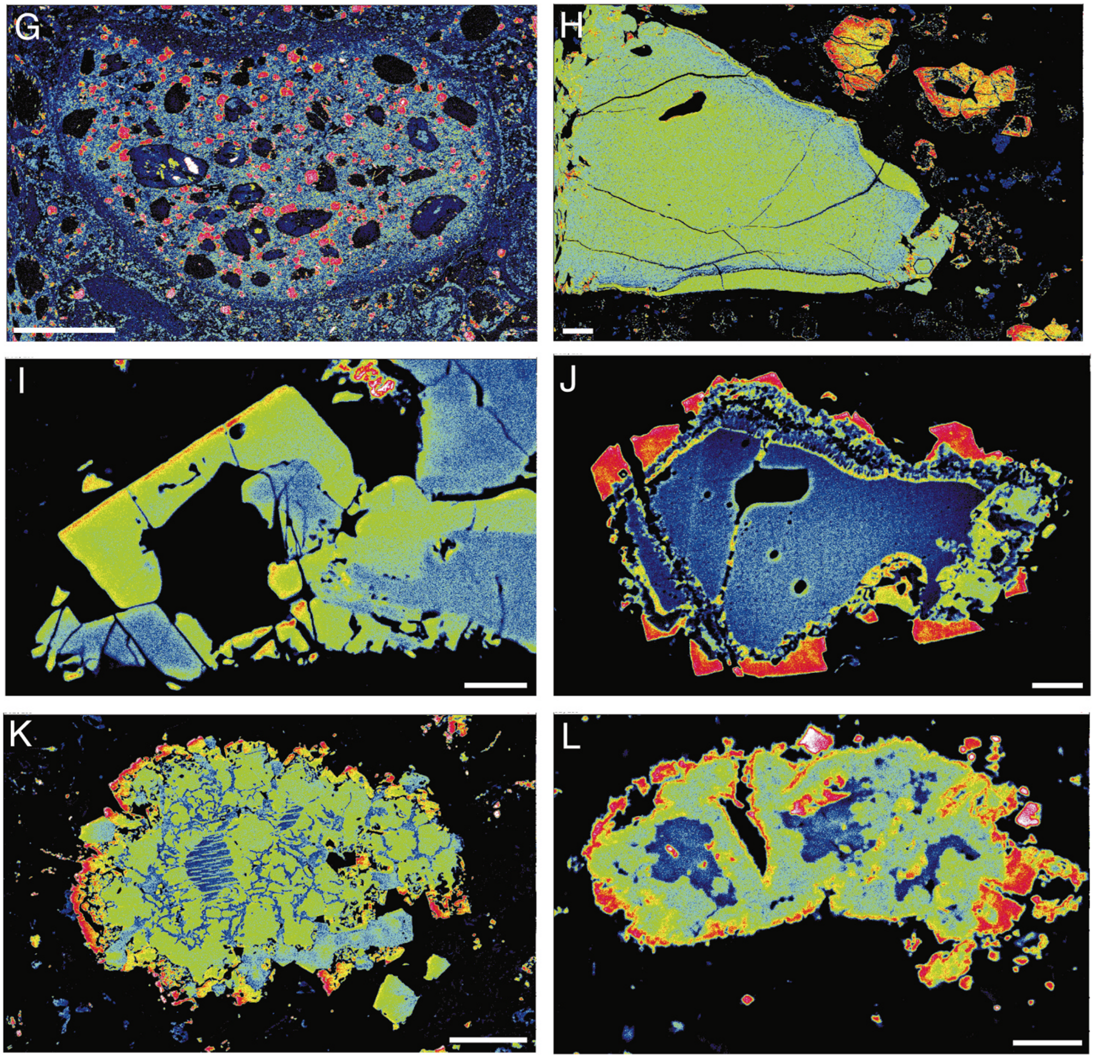

(striped blue) successively rimmed by MUM spinel (green), perovskite (greenish blue) and titaniferous magnetite (orange). Wesselton Sill, South Africa. (L) Priderite (blue) rimmed by perovskite (green) with a *REE*–Na–Nb-enriched rim (red). Lac de Gras, NWT.

intermediate zone consisting of very fine-grained calcite, commonly in association with serpentine. A morphological resemblance between such aggregates and atoll spinels (Fig. 3B) probably reflects their simultaneous formation during interaction of the primary oxide minerals, *i.e.*, perovskite and spinels, with a CO_2-rich fluid. During the subsequent evolution of kimberlite, the space between the core and rim may be filled with late-stage minerals such as barite (Fig. 3C). According to Mitchell & Clarke (1976), pseudomorphs after perovskite from Peuyuk (Nunavut) exhibit a zone of nickeliferous pyrite between a perovskite core and a TiO_2 rim. It is unclear, however, whether pyrite formed prior to TiO_2 or, in common with barite, after the atoll rim had developed (see below).

In some kimberlites (*e.g.*, Chomur in Yakutia and Iron Mountain in Wyoming), the reaction-induced rim on perovskite consists of TiO_2 intimately intergrown with titanite (Mitchell & Chakhmouradian 1998a). Such intergrowths typically have a lamellar texture indicating that the two minerals crystallized in equilibrium (Fig. 3D). Titanite is generally atypical of kimberlites, its precipitation indicating some increase in $a(SiO_2)$ during the replacement stage due to contamination of

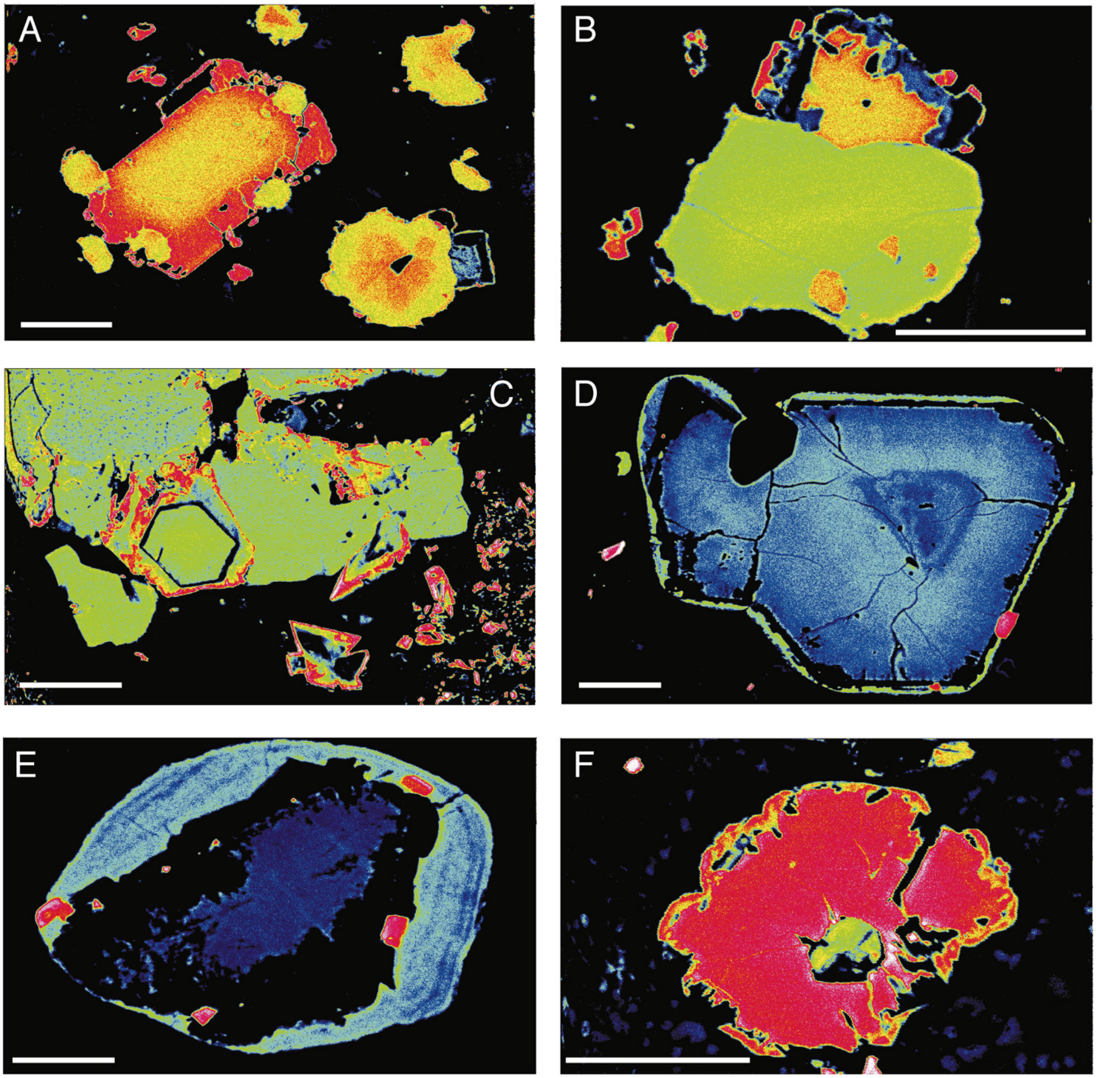

FIG. 2. Relationships of perovskite with other Ti-bearing oxide phases in kimberlites. False-color BSE images. Scale bar is 20 μm for all images. (A) Primitively zoned perovskite crystals (orange to yellow) partly enclosed within a MUM spinel (orange) rimming chromite core (yellow). Matsoku, Lesotho. (B) Perovskite crystal (green) with inclusions of magnesiochromite (orange) intergrown with an atoll spinel. Note that the atoll rim is present only where the spinel is not bordered by perovskite. Matsoku, Lesotho. (C) Atoll spinel (euhedral green, with a red rim) completely enclosed by a reaction-induced rim of perovskite on macrocrystic ilmenite. Detail of Figure 1H. Premier mine, South Africa. (D) Euhedral crystal of perovskite (red) enclosed in the atoll rim (green) of a zoned spinel crystal (blue). Lac de Gras, NWT. (E) Atoll spinel with a strongly resorbed core (dark blue) and subhedral inclusions of perovskite (red) in a rim (pale blue). Lac de Gras, NWT. (F) Euhedral inclusion of geikielite (green) in perovskite (red) rimmed by TiO_2 (orange red). Tunraq, Nunavut.

kimberlite with material from the upper crust. This process can be described by the following reaction scheme:

$$2CaTiO_3 + CO_2 + (SiO_2)_{aq} \Leftrightarrow TiO_2 + CaTiSiO_5 + CaCO_3 \quad (2)$$

In multicomponent pseudomorphs, TiO_2 and titanite are typically succeeded by ilmenite, the second most common product of perovskite alteration in kimberlites. In some kimberlites, all intermediate stages of successive replacement of perovskite by TiO_2 and, then, by ilmenite can be observed within one thin section (Chomur: Figs. 3D–F). The crystallization of ilmenite reflects an increase in $a(Fe^{2+})$, $a(Mn^{2+})$ and, in some cases, $a(Mg^{2+})$ at the final stages of perovskite alteration (Mitchell & Chakhmouradian 1998a). Under high $P(H_2S)$, an increase in $a(Fe^{2+})$ may lead to the replacement of TiO_2 by pyrite, as observed in sulfide-rich kimberlites such as Peuyuk C (Fig. 3G).

In some occurrences, *e.g.*, Tunraq (Nunavut) and Chicken Park (Colorado), reaction-induced rims are composed entirely of ilmenite, and lack TiO_2, titanite or other intermediate products of perovskite alteration. The ilmenite rims are typically discontinuous and vary from a few μm to 60 μm in thickness (Figs. 3H, I). In most cases, ilmenite developed on perovskite is enriched in Mn (up to 31 mol.% $MnTiO_3$), and depleted in Mg (<2 mol.% $MgTiO_3$), Cr and Fe^{3+}. In terms of composition, this mineral is very distinct from macrocrystic and microcrystic ilmenite, and belongs to the so-called reaction or manganese-enrichment trend (Mitchell 1986). One of a few exceptions is to be found in the Chomur kimberlite, in which ilmenite is relatively poor in Mn (<6 mol.% $MnTiO_3$), and abnormally enriched in Mg (22–28 mol.% $MgTiO_3$) (Figs. 3E, F). Regardless of the Mg:Mn ratio, ilmenite in the reaction-induced rims is poor in Fe^{3+} (<1.6 wt.% Fe_2O_3), practically devoid of Cr (<0.2 wt.% Cr_2O_3), and typically contains appreciable Nb (up to 1.1 wt.% Nb_2O_5). The replacement of perovskite by ilmenite can be described by the following reaction scheme:

$$CaTiO_3 + (1 - n)Fe^{2+} + nMn^{2+} \Leftrightarrow Fe_{1-n}Mn_nTiO_3 + Ca^{2+} \quad (3)$$

In kimberlite from Premier (South Africa), perovskite underwent replacement by titaniferous magnetite (Fig. 3J). The alteration process culminated with the formation of zoned pseudomorphs consisting of relict perovskite in the core, an intermediate zone, and magnetite in the rim (Fig. 3K). In the intermediate zone, the proportion of the major elements Ca:Ti:Fe is fairly consistent and approaches 1:1:3, suggesting that this zone is composed of perovskite ($CaTiO_3$) and nearly pure magnetite (Fe_3O_4) in almost equal proportions. In our opinion, that this represents a single phase such as $CaTiFe_3O_{6+\delta}$ ($\delta = ½Fe^{3+}$) should be ruled out because, in the given compositional range, perovskite and spinel (± ilmenite) are stable oxide phases under reducing conditions (Kimura & Muan 1971). Also, such hypothetical Ca–Ti-ferrite compounds have been neither synthesized nor observed in nature. We are uncertain, however, whether cryptocrystalline perovskite and magnetite are the only components of this replacement assemblage. The consistency of the Ca:Ti:Fe proportions in the intermediate zone indicates that, if present, other oxide phases (*e.g.*, ilmenite) occur here in relatively minor amounts. The outermost zone of pseudomorphs consists of titaniferous magnetite of the approximate composition $Mgt_{72}Usp_{12}Qnd_8Spl_8$.

In some occurrences, perovskite crystals exhibit a pseudo-atoll texture created by a thin rim of magnetite encircling a perovskite core. However, a close examination of such intergrowths shows that the magnetite rim developed on grains of spinel "welded" to the perovskite core, rather than on perovskite itself (Fig. 3L). Consequently, the formation of the atoll rim of magnetite in such cases does not manifest the alteration of perovskite.

Rarely, perovskite in kimberlites undergoes a more complex succession of replacement reactions, giving rise to intricate pseudomorphs consisting of four or more secondary phases. For example, at Iron Mountain (Wyoming), perovskite first underwent cation leaching and conversion to cassite, $CaTi_2O_4(OH)_2$ (Fig. 3M). Subsequently, cassite and relict fragments of perovskite were further replaced by anatase, calcite and minor titanite. This assemblage, in its turn, became unstable and was partly replaced by Mn-rich ilmenite. At the final stages of the alteration process, the light rare-earth elements (*LREE*) released from the primary perovskite were redeposited in the form of lucasite-(Ce), $CeTi_2O_5(OH)$ (Fig. 3N).

The above-described alteration patterns have been observed only in hypabyssal and diatreme-facies kimberlites. Resorption, cation leaching and replacement of perovskite by other minerals are characteristically absent in crater-facies rocks.

COMPOSITIONAL VARIATION

All mineral compositions were determined by X-ray energy-dispersion spectrometry (EDS) using a Hitachi 570 scanning electron microscope equipped with a LINK ISIS analytical system incorporating a Super ATW Light Element Detector (133 eV FwHm Mn_K) at Lakehead University, Ontario. EDS spectra of perovskite were acquired for 130 seconds (live time) with an accelerating voltage of 20 kV and a beam current of 0.84–0.85 nA. X-ray spectra were collected and processed with the LINK ISIS–SEMQUANT software package. Full ZAF corrections were applied to the raw X-ray data. The following standards were used for the determination of mineral compositions: loparite (Na, La, Ce, Pr, Nd, Nb), perovskite (Ca, Ti, Fe), synthetic $SrTiO_3$ (Sr), wollastonite (Si), corundum (Al), metallic

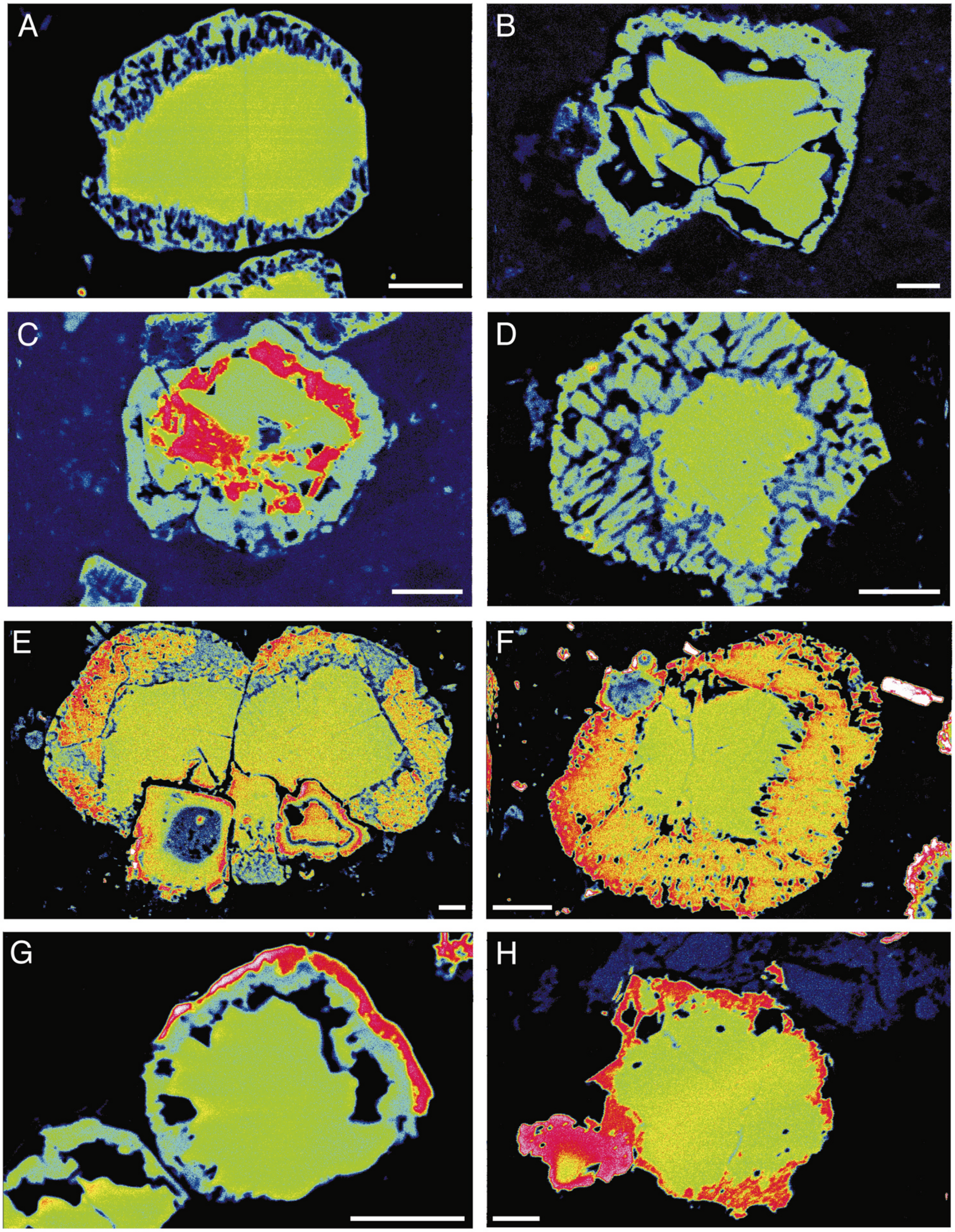

FIG. 3. Characteristic alteration patterns of perovskite in kimberlites. False-color BSE images. Scale bar is 10 μm for images A–J,L and N, and 40 μm for K and M. (A) "Spongy" reaction-induced rim of TiO_2 (bluish green) on perovskite. Peuyuk C, Nunavut. (B–C). Atoll-textured grains of perovskite with a rim of TiO_2. In (C), the "lagoon" is filled with barite (red). Peuyuk B, Nunavut. (D–F). Successive stages of replacement of perovskite (green, yellowish green) by TiO_2 (bluish green) and

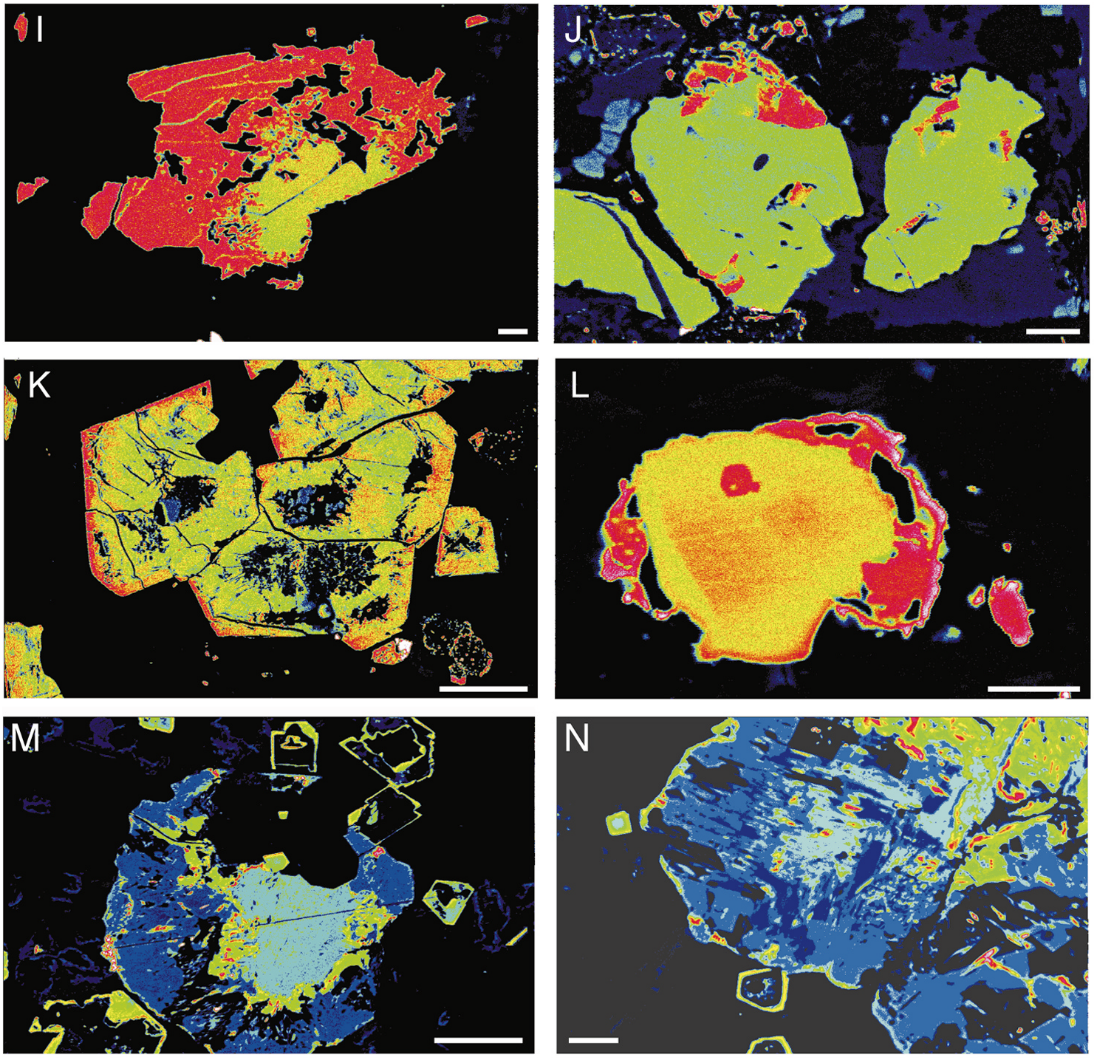

magnesian ilmenite (orange). TiO_2 in the replacement rim is associated with minor titanite and calcite. On (E) and (F), perovskite is intergrown with smaller spinel crystals (blue to red). Chomur, Yakutia. (G). Successive rimming of perovskite (green) by TiO_2 (bluish green) and pyrite (red). Peuyuk C, Nunavut. (H–I) Reaction-induced rim of ilmenite (red) on perovskite (yellowish green). Other minerals are chromite (yellow) rimmed by MUM spinel (purple), and apatite (blue). Chicken Park, Colorado. (J) Incipient replacement of perovskite (green) by titaniferous magnetite (red). Blue is apatite. Premier mine, South Africa. (K) Complex pseudomorphs of magnetite (green to red) after perovskite (blue). Premier mine, South Africa. (L) Perovskite with a pseudo-atoll texture. Note that the atoll rim (purple) is present only where perovskite (yellow) is integrown with MUM spinel (red). Matsoku, Lesotho. (M–N) Complex pseudomorphs after perovskite consisting of kassite (pale blue), anatase (blue) and Mn-rich ilmenite (green). Note that on (N), anatase is intimately intergrown with titanite (dark blue), and fractures host minute crystals of lucasite (red). Iron Mountain, Wyoming.

Th, Zr and Ta. The accuracy of this method was cross-checked by wavelength-dispersion electron-microprobe analysis on an automated CAMECA SX–50 instrument using a zoned crystal of perovskite from the Hills Pond lamproite (Mitchell & Chakhmouradian 1999). Representative compositions of perovskite from twenty-one kimberlite localities worldwide are given in Tables 1–6.

In back-scattered electron images (BSE), discrete crystals of perovskite typically exhibit a simple pattern of zonation, with a bright core and a comparatively

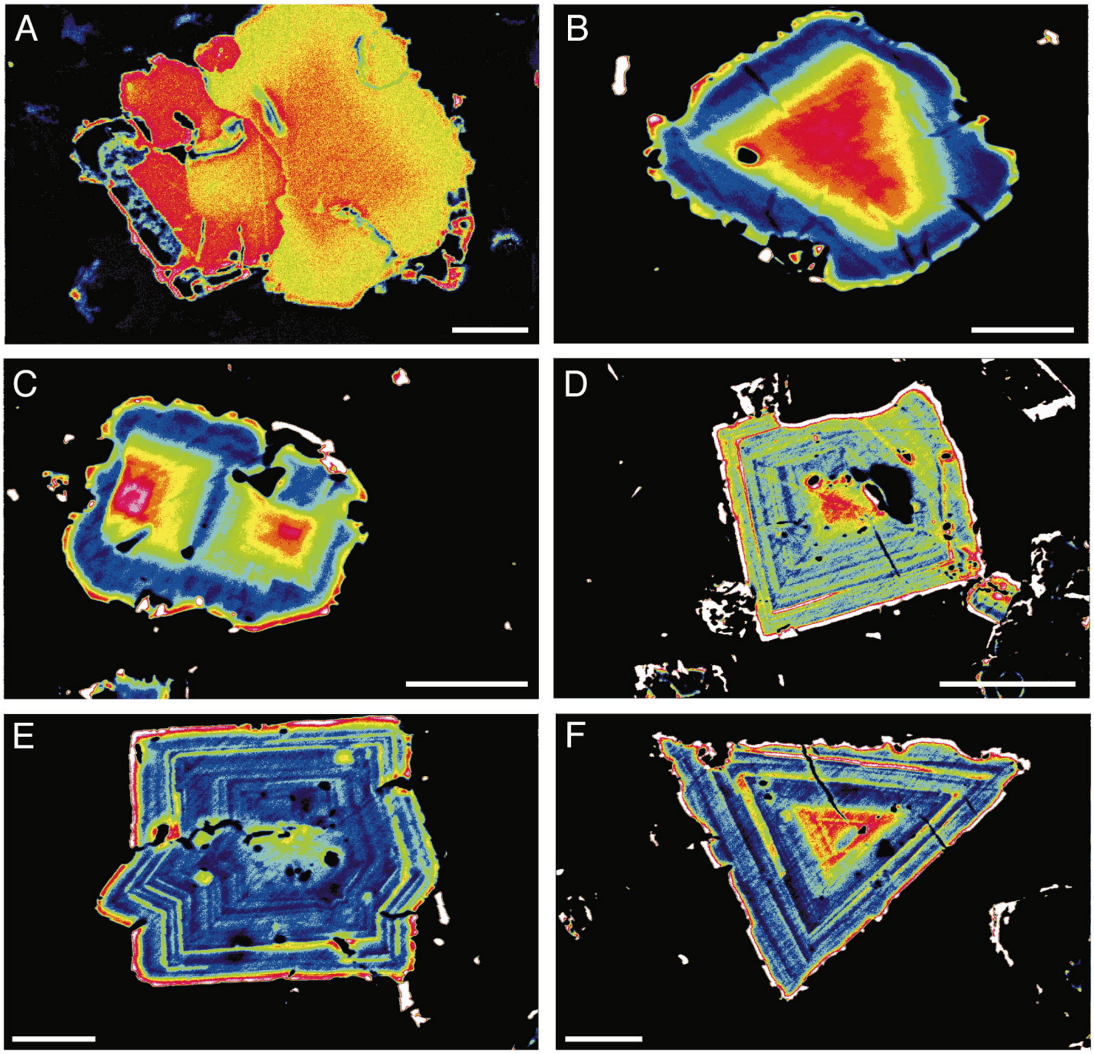

FIG. 4. Characteristic zonation patterns of perovskite in kimberlites. False-color BSE images. Scale bar is 10 μm for all images. (A) Primitively zoned perovskite with *REE*, Th, Na and Nb contents decreasing toward the rim. Matsoku, Lesotho. (B–C) Perovskite with a normal pattern of zonation and several transitional zones. Wesselton mine, South Africa. (E–F) Perovskite with oscillatory pattern of zonation. Benfontein mine, South Africa.

darker rim (Fig. 4A). In most cases, the difference in brightness between the core and rim is created by variations in *LREE*, Th and Nb contents. From the core outward, discrete crystals of perovskite with simple zonation typically show some decrease in *LREE* and Th, which may or may not be accompanied by declining Nb and Na contents (*e.g.*, Table 1, anal. 1–2, and Table 5, anal. 6–7). In zoned perovskite from the Kirkland Lake area (Ontario), the *LREE*, Th and Na contents decrease, whereas the concentrations of Nb and Fe increase toward the rim (Table 6, anal. 5–6). As *LREE* and Th have the most consistent behavior among the minor elements, we further refer to the above-described type of zonation as a normal pattern of zonation (Fig. 4A). Such a normal pattern may be complicated by the presence of several transitional zones with intermediate *LREE* contents (Fig. 4B), or by the coexistence of two or more nuclei within the same crystal (Fig. 4C). A reversed pattern of zonation, *i.e.*, that involving an increase in *LREE* and Th toward the rim, is much less common in kimberlites, and most probably results from re-equilibration of perovskite with a magma modified by assimilation or contamination processes (Fig. 1L).

TABLE 1. REPRESENTATIVE COMPOSITIONS OF PEROVSKITE FROM KIMBERLITES. AFRICAN OCCURRENCES

Wt.%	1	2	3	4	5	6	7	8	9	10
Na_2O	0.88	0.42	0.60	0.16	0.82	0.68	0.40	0.12	0.36	0.63
CaO	36.00	39.02	38.72	40.19	34.79	35.68	37.73	38.90	39.42	39.20
SrO	0.33	0.34	0.27	0.31	0.24	0.46	0.27	0.37	0.27	0.18
La_2O_3	0.95	0.38	0.02	n.d	2.24	1.41	0.79	0.79	n.d	0.19
Ce_2O_3	2.91	0.89	1.23	0.21	4.42	2.86	2.39	1.46	n.d	0.93
Pr_2O_3	0.27	n.d	n.d	n.d	0.47	0.69	n.d	n.d	n.d	n.d
Nd_2O_3	0.68	n.d	0.13	n.d	1.35	1.39	0.59	0.22	n.d	n.d
ThO_2	0.81	n.d	0.36	n.d	1.04	0.10	n.d	n.d	0.09	n.d
TiO_2	53.82	55.28	57.28	57.59	52.97	52.80	54.80	55.55	57.46	57.46
Al_2O_3	n.d	n.d	n.d	n.d	n.d	n.d	0.36	0.29	n.d	n.d
Fe_2O_3*	1.00	1.31	0.86	1.22	2.28	1.76	1.53	1.39	0.91	0.82
Nb_2O_5	1.03	0.75	0.46	0.31	0.71	0.92	0.83	0.70	0.28	0.60
Ta_2O_5	0.39	0.46	0.45	0.29	n.d	n.d	0.23	0.31	n.d	0.49
Total	99.07	98.85	100.38	100.28	101.33	98.75	99.92	100.10	98.79	100.68
Structural formulae based on 3 atoms of oxygen										
Na	0.041	0.019	0.027	0.007	0.038	0.032	0.018	0.005	0.016	0.028
Ca	0.917	0.973	0.949	0.978	0.885	0.917	0.941	0.962	0.971	0.955
Sr	0.005	0.005	0.004	0.004	0.003	0.006	0.004	0.005	0.004	0.002
La	0.008	0.003	-	-	0.020	0.012	0.007	0.007	-	0.002
Ce	0.025	0.008	0.010	0.002	0.038	0.025	0.020	0.012	-	0.008
Pr	0.002	-	-	-	0.004	0.006	-	-	-	-
Nd	0.006	-	0.001	-	0.011	0.012	0.005	0.002	-	-
Th	0.004	-	0.002	-	0.006	0.001	-	-	-	-
$\sum A$	1.008	1.008	0.993	0.991	1.005	1.011	0.995	0.993	0.991	0.995
Ti	0.963	0.968	0.985	0.984	0.946	0.952	0.959	0.964	0.993	0.985
Al	-	-	-	-	-	-	0.010	0.008	-	-
Fe	0.018	0.023	0.015	0.021	0.041	0.032	0.027	0.024	0.016	0.014
Nb	0.011	0.008	0.005	0.003	0.008	0.010	0.009	0.007	0.003	0.006
Ta	0.003	0.003	0.003	0.002	-	-	0.001	0.002	-	0.003
$\sum B$	0.995	1.002	1.008	1.010	0.995	0.994	1.006	1.005	1.012	1.008
Mol.% end-members										
$NaNbO_3$	1.34	1.07	0.75	0.50	0.75	0.99	1.02	0.54	0.30	0.94
Loparite	5.33	1.62	3.80	0.42	5.96	4.28	1.58	-	-	1.57
$CeFeO_3$	1.46	0.27	-	-	4.30	3.35	2.43	2.10	-	0.16
$CaTiO_3$	90.56	96.58	94.72	98.67	87.55	90.64	94.60	96.86	99.24	97.09
$SrTiO_3$	0.45	0.46	0.36	0.41	0.33	0.63	0.37	0.50	0.37	0.24
$Th_{0.5}TiO_3$	0.86	-	0.37	-	1.11	0.11	-	-	0.09	-

1-2 core and rim of a zoned crystal, respectively, Matsoku (Lesotho); 3-4 core and rim of a weakly zoned crystal, respectively, Thaba Putsoa (Lesotho); 5-6 core and rim of a zoned crystal, respectively, Wesselton mine (South Africa); 7-8 Wesselton Sill (South Africa); 9-10 Premier (South Africa): 9 reaction-induced rim on macrocrystal geikielite, 10 discrete crystal in groundmass. * Total Fe as Fe_2O_3; n.d = not detected. Loparite = $Na_{0.5}Ce_{0.5}TiO_3$.

Oscillatory zonation is relatively uncommon in perovskite from kimberlites. It typically involves only subtle variations in Ca, Ti, *LREE* and other minor components on a very fine scale. In most cases, an oscillatory zonation is difficult to detect with relatively low beam currents employed in the SEM–EDS routine. One of the best examples of oscillatory zonation can be seen in perovskite from the Benfontein sill in South Africa. Some perovskite crystals from this locality consist of more than 25 individual zones ranging from 0.2 to 3 μm in thickness (Figs. 4D–F). The difference in contrast between the individual zones in this mineral is largely due to variations in the Nb (0.8–3.1 wt.% Nb_2O_5), *LREE* (4.1–7.4 wt.% $LREE_2O_3$) and, to a lesser extent, Th contents (0–1.7 wt.% ThO_2).

The analytical data obtained in the present study show that perovskite from kimberlites is close to the ideal composition $CaTiO_3$, and has relatively minor contents of substituting elements (*LREE*, Na, Sr, Th, Si, Zr, Al, Fe, Nb and Ta), especially in comparison with perovskite-group minerals from evolved alkaline rocks (Chakhmouradian & Mitchell 1997, 1998, Mitchell & Chakhmouradian 1999). The light lanthanides, Na, Th, Nb and Fe demonstrate the most significant variation in

TABLE 2. REPRESENTATIVE COMPOSITIONS OF PEROVSKITE FROM KIMBERLITES. AFRICAN OCCURRENCES

Wt.%	1	2	3	4	5	6
Na_2O	0.61	0.49	0.36	0.30	0.96	0.50
CaO	34.48	35.49	38.88	38.93	34.56	37.44
SrO	0.49	0.20	0.17	0.36	0.32	0.20
La_2O_3	1.24	1.58	0.72	0.41	1.61	0.97
Ce_2O_3	3.36	3.80	1.50	1.01	3.93	1.80
Pr_2O_3	n.d	0.42	n.d	n.d	0.19	0.34
Nd_2O_3	1.02	1.39	0.24	n.d	0.50	0.35
ThO_2	0.64	0.43	0.13	n.d	0.45	n.d
TiO_2	50.65	52.33	55.75	55.78	53.56	55.06
Al_2O_3	n.d	0.38	n.d	n.d	n.d	n.d
Fe_2O_3*	1.72	1.69	0.97	1.18	1.32	1.20
Nb_2O_5	3.09	1.64	0.15	0.58	0.99	0.48
Ta_2O_5	0.84	0.36	0.33	0.20	n.d	n.d
Total	98.14	100.20	99.20	98.75	98.39	98.34
Structural formulae based on 3 atoms of oxygen						
Na	0.029	0.023	0.016	0.014	0.045	0.023
Ca	0.898	0.904	0.970	0.970	0.889	0.945
Sr	0.007	0.003	0.002	0.005	0.004	0.003
La	0.011	0.014	0.006	0.003	0.014	0.008
Ce	0.030	0.033	0.013	0.009	0.035	0.016
Pr	-	0.004	-	-	0.002	0.003
Nd	0.009	0.012	0.002	-	0.004	0.003
Th	0.004	0.002	0.001	-	0.002	-
$\sum A$	0.988	0.995	1.010	1.001	0.995	1.001
Ti	0.926	0.936	0.976	0.975	0.967	0.976
Al	-	0.011	-	-	-	-
Fe	0.031	0.030	0.017	0.021	0.024	0.021
Nb	0.034	0.018	0.002	0.006	0.011	0.005
Ta	0.006	0.002	0.002	0.001	-	-
$\sum B$	0.997	0.997	0.997	1.003	1.002	1.002
Mol.% end-members						
$NaNbO_3$	2.90	2.00	0.36	0.74	1.08	0.51
Loparite	-	0.53	2.49	1.23	6.80	3.55
$CeFeO_3$	5.04	6.00	0.83	0.60	2.09	1.21
$CaTiO_3$	90.64	90.72	95.95	96.95	89.09	94.46
$SrTiO_3$	0.70	0.28	0.23	0.48	0.45	0.27
$Th_{0.5}TiO_3$	0.72	0.47	0.14	-	0.49	-

1-2 oscillatory-zoned crystal, Benfontein (South Africa); 3-4 Ondermatje (South Africa); 5-6 core and rim of a zoned crystal, Frank Smith mine (South Africa). * Total Fe as Fe_2O_3; n.d not detected. Loparite = $Na_{0.5}Ce_{0.5}TiO_3$.

concentration, both on a macro-scale, *i.e.*, among different kimberlite provinces and intrusions, and on a micro-scale, corresponding to intragranular zonation. Among the samples studied, the highest concentrations of *LREE*, Nb and Fe^{3+} (up to 11.1, 8.6 and 5.6 wt.% of the respective oxides) are observed in perovskite from the Lac de Gras kimberlite field (NWT). Perovskite from some intrusions at Lac de Gras is also enriched in Na, Th, Zr and Al (Table 5, anal. 1–3). Some enrichment in Na, *LREE*, Th, Nb and Fe^{3+} (up to 1.6, 9.4, 1.8, 3.8 and 2.6 wt.% of the respective oxides) is characteristic of small zoned crystals of perovskite from the Kirkland Lake area (Table 6, anal. 5–6). At Fort à la Corne (Saskatchewan), perovskite contains noticeable concentrations of *LREE* (3.8–10.1 wt.% $LREE_2O_3$) and Th (up to 2.2 wt.% ThO_2), but has "normal" levels of Na, Fe and Nb (Table 4, anal. 7–12). Complexly zoned crystals of perovskite from Obnazhennaya (Yakutia) and Benfontein are locally enriched in Nb (up to 5.2 and 3.1 wt.% Nb_2O_5, respectively) and *LREE* (up to 9.8 and 7.2 wt.% $LREE_2O_3$, respectively). These examples of perovskite enriched in incompatible elements show no obvious correlation with a particular kimberlite facies or mineral paragenesis. At Lac de Gras, both hypabyssal and crater-facies kimberlites contain *LREE*–Nb–Fe-rich perovskite. The samples from Fort à la Corne are crater-facies rocks, whereas those from Benfontein and Obnazhennaya are hypabyssal kimberlites. At Obnazhennaya, the *LREE*–Nb-enriched perovskite occurs in a calcite – serpentine groundmass of a primitive macrocryst-rich kimberlite, in association with Nb-rich pyrophanite. The Benfontein sample examined in the present work is a differentiated calcite- and apatite-rich kimberlite containing layers enriched in spinel-group minerals, perovskite and baddeleyite. In contrast to Benfontein, well-differentiated hypabyssal kimberlites from Wesselton sill (South Africa) contain perovskite with unremarkable Nb, *LREE* and Th contents (Table 1, anal. 7–8).

In order to facilitate comparison of perovskite from kimberlites and other rock types, we recalculated the compositions obtained in the present study to end-mem-

TABLE 3. REPRESENTATIVE COMPOSITIONS OF PEROVSKITE FROM KIMBERLITES. ASIAN OCCURRENCES

Wt.%	1	2	3	4	5	6	7	8	9
Na_2O	2.00	1.47	1.74	0.42	0.38	0.35	0.31	0.40	0.08
CaO	29.59	34.15	33.45	38.58	39.92	35.12	37.08	34.19	37.94
SrO	0.24	0.33	0.24	0.28	0.25	0.37	0.57	0.39	0.77
La_2O_3	2.15	1.32	2.41	0.50	0.59	1.98	1.71	2.72	1.41
Ce_2O_3	5.36	3.59	5.12	1.64	0.92	3.85	2.61	4.82	1.67
Pr_2O_3	0.50	0.25	n.d	n.d	n.d	0.88	0.31	0.80	0.54
Nd_2O_3	1.80	0.89	0.61	0.33	n.d	1.55	1.26	1.35	0.50
ThO_2	2.71	0.10	0.14	0.16	n.d	0.85	n.d	0.77	n.d
TiO_2	47.75	51.41	50.79	56.82	57.62	52.71	54.46	52.49	53.81
SiO_2	0.16	0.27	0.34	n.d	n.d	n.d	n.d	n.d	n.d
Fe_2O_3*	1.66	1.73	1.69	1.07	1.12	1.81	1.91	2.00	2.19
Nb_2O_5	5.22	3.31	4.37	0.35	0.45	0.65	0.39	0.62	0.82
Ta_2O_5	1.02	n.d	n.d	0.06	0.30	n.d	n.d	n.d	n.d
Total	100.16	98.82	100.90	100.21	101.55	100.12	100.61	100.55	99.73
Structural formulae based on 3 atoms of oxygen									
Na	0.096	0.068	0.080	0.019	0.017	0.016	0.014	0.019	0.004
Ca	0.786	0.876	0.853	0.951	0.967	0.902	0.930	0.881	0.954
Sr	0.003	0.005	0.003	0.004	0.003	0.005	0.008	0.005	0.010
La	0.020	0.012	0.021	0.004	0.005	0.018	0.015	0.024	0.012
Ce	0.049	0.032	0.045	0.014	0.008	0.034	0.022	0.042	0.014
Pr	0.005	0.002	-	-	-	0.008	0.003	0.007	0.005
Nd	0.016	0.008	0.005	0.003	-	0.013	0.011	0.012	0.004
Th	0.015	0.001	0.001	0.001	-	0.005	-	0.004	-
$\sum A$	0.990	1.004	1.008	0.996	1.000	1.001	1.003	0.994	1.003
Ti	0.890	0.927	0.909	0.983	0.979	0.950	0.959	0.949	0.950
Si	0.004	0.006	0.008	0.983	0.979	0.950	0.959	0.949	0.950
Fe	0.031	0.031	0.030	0.019	0.019	0.033	0.034	0.036	0.039
Nb	0.059	0.036	0.047	0.004	0.005	0.007	0.004	0.007	0.009
Ta	0.007	-	-	-	0.002	-	-	-	-
$\sum B$	0.991	1.000	0.994	1.006	1.005	0.990	0.997	0.992	0.998
Mol.% end-members									
$NaNbO_3$	6.51	3.57	4.66	0.40	0.64	0.70	0.41	0.68	0.36
Loparite	6.12	6.46	6.59	2.96	2.04	1.84	1.98	2.39	-
$CeFeO_3$	5.77	2.05	3.74	0.61	0.23	6.27	4.03	7.34	3.52
$CaTiO_3$	78.22	87.35	84.53	95.49	96.75	89.76	92.81	88.21	95.08
$SrTiO_3$	0.34	0.46	0.33	0.38	0.33	0.51	0.77	0.54	1.04
$Th_{0.5}TiO_3$	3.04	0.11	0.15	0.17	-	0.92	-	0.84	-

1-3 Obnazhennaya (Yakutia, Russia): 1-3 core, intermediate zone and rim of a zoned crystal, respectively, 4 unzoned crystal; 5-6 Chomur (Yakutia, Russia); 7-10 Xi-Yu (China): 7-8 and 9-10 core and rim of two zoned crystals, respectively. * Total Fe as Fe_2O_3; n.d = not detected. Loparite = $Na_{0.5}Ce_{0.5}TiO_3$.

TABLE 4. REPRESENTATIVE COMPOSITIONS OF PEROVSKITE FROM KIMBERLITES. NORTH AMERICAN OCCURRENCES

Wt.%	1	2	3	4	5	6	7	8	9	10	11	12
Na_2O	0.43	0.22	0.44	1.05	0.84	0.62	0.41	0.86	0.42	0.28	0.44	0.34
CaO	35.99	40.00	38.28	34.26	36.03	36.53	36.68	34.41	37.64	35.40	35.75	34.25
SrO	0.31	0.44	0.29	0.41	0.20	0.36	0.20	0.20	0.04	0.38	0.37	0.27
La_2O_3	1.09	0.69	0.82	1.64	1.22	1.67	1.15	1.49	1.24	1.38	1.10	1.57
Ce_2O_3	2.37	0.96	2.02	3.68	3.25	3.38	3.17	4.18	2.90	4.12	3.55	4.96
Pr_2O_3	0.59	n.d	n.d	0.55	0.38	0.23	0.33	n.d	n.d	0.18	0.05	0.46
Nd_2O_3	0.77	n.d	0.16	1.12	0.95	1.00	0.78	1.24	0.62	0.96	1.00	1.48
ThO_2	0.17	n.d	0.24	0.56	0.44	0.70	n.d	2.19	0.03	1.11	0.98	1.02
TiO_2	53.40	55.64	56.63	52.37	53.55	54.47	53.78	52.85	54.61	53.71	53.52	50.48
Al_2O_3	n.d	0.40	n.d	n.d	0.34	0.23	0.36	0.30	0.24	0.64	0.56	0.75
Fe_2O_3*	1.89	1.79	1.12	1.78	1.45	1.28	1.30	1.36	1.22	1.42	1.59	2.50
Nb_2O_5	0.86	0.56	0.50	2.07	0.97	0.75	1.52	1.81	1.36	0.68	0.74	1.32
Ta_2O_5	0.32	0.16	0.24	0.24	0.37	0.34	0.20	0.46	0.03	0.31	0.37	0.41
Total	98.19	100.86	99.41	99.73	99.99	101.56	99.88	101.35	100.35	100.57	100.02	99.81
Structural formulae based on 3 atoms of oxygen												
Na	0.020	0.010	0.020	0.049	0.038	0.028	0.019	0.040	0.019	0.013	0.020	0.016
Ca	0.922	0.978	0.943	0.879	0.912	0.913	0.924	0.874	0.939	0.896	0.906	0.887
Sr	0.004	0.006	0.005	0.006	0.003	0.005	0.003	0.003	0.001	0.005	0.005	0.004
La	0.010	0.006	0.007	0.014	0.011	0.014	0.010	0.013	0.011	0.012	0.010	0.014
Ce	0.021	0.008	0.017	0.032	0.028	0.029	0.027	0.036	0.025	0.036	0.031	0.044
Pr	0.005	-	-	0.005	0.003	0.002	0.003	-	-	0.002	-	0.004
Nd	0.007	-	0.001	0.010	0.008	0.008	0.007	0.011	0.005	0.008	0.008	0.013
Th	0.001	-	0.001	0.003	0.002	0.004	-	0.012	-	0.006	0.005	0.006
$\sum A$	0.990	1.008	0.994	0.998	1.005	1.003	0.993	0.989	1.000	0.978	0.985	0.989
Ti	0.960	0.955	0.979	0.943	0.952	0.957	0.951	0.943	0.956	0.954	0.952	0.917
Al	-	0.011	-	-	0.009	0.006	0.010	0.008	0.007	0.018	0.016	0.021
Fe	0.034	0.031	0.019	0.032	0.026	0.022	0.023	0.024	0.021	0.025	0.028	0.045
Nb	0.009	0.006	0.005	0.022	0.010	0.008	0.016	0.019	0.014	0.007	0.008	0.014
Ta	0.002	0.001	0.002	0.002	0.002	0.002	0.001	0.003	-	0.002	0.002	0.003
$\sum B$	1.005	1.004	1.005	0.999	0.999	0.995	1.001	0.997	0.998	1.006	1.006	1.000
Mol.% end-members												
$NaNbO_3$	1.15	0.67	0.67	2.40	1.26	1.00	1.76	2.24	1.45	0.94	1.04	1.72
Loparite	1.73	0.59	2.60	4.95	5.11	3.57	0.25	3.43	0.89	0.73	2.00	-
$CeFeO_3$	3.39	1.08	1.24	3.63	2.41	3.53	4.58	4.27	3.61	5.47	3.97	7.62
$CaTiO_3$	93.12	97.08	94.84	87.84	90.48	90.68	93.14	87.42	93.97	91.12	91.42	89.15
$SrTiO_3$	0.43	0.58	0.39	0.57	0.27	0.48	0.28	0.28	0.05	0.53	0.51	0.38
$Th_{0.5}TiO_3$	0.19	-	0.25	0.61	0.47	0.74	-	2.36	0.03	1.21	1.06	1.13

1 relict perovskite fragment in a core of kassite-anatase-ilmenite pseudomorph, Iron Mountain (Wyoming, U.S.A.); 2-3 discrete unzoned crystals from different intrusions, Chicken Park (Colorado, U.S.A.); 4-6 northwestern Alberta (Canada): 4 reaction-induced rim on microcrystal geikielite, 5-6 discrete unzoned crystal from different intrusions; 7-12 Fort à la Corne (Saskatchewan, Canada): 7 overgrowth on macrocrystal geikielite, 8-12 discrete unzoned crystals from different intrusions. * Total Fe as Fe_2O_3; n.d = not detected. Loparite = $Na_{0.5}Ce_{0.5}TiO_3$.

ber components, following recommendations of Mitchell (1996) and Mitchell & Chakhmouradian (1998b). In addition to the conventionally used end-members, *i.e.*, $CaTiO_3$, $SrTiO_3$, $Na_{0.5}Ce_{0.5}TiO_3$, $NaNbO_3$ and $Th_{0.5}TiO_3$, we introduced the component $CeFeO_3$ into the recalculation scheme to account for *LREE* left unassigned after subtraction of the loparite component $Na_{0.5}Ce_{0.5}TiO_3$, and for the trivalent *B*-site cations (Fe and minor Al). For perovskite from Lac de Gras, which shows the maximum enrichment in incompatible elements and Al, the end-members $CaFe_{0.5}Nb_{0.5}O_3$ (latrappite) and $CaZrO_3$ were also included in the recalculation procedure. The latrappite component in the Lac de Gras perovskite accounts for the Nb and trivalent cations not incorporated in $NaNbO_3$ and $CeFeO_3$, respectively. The results of recalculations presented in Tables 1–6 demonstrate that, in most kimberlite occurrences, perovskite contains more than 90 mol.% $CaTiO_3$. The amount of any of the minor components typically does not exceed 7 mol.%. Lueshite ($NaNbO_3$), loparite ($Na_{0.5}Ce_{0.5}TiO_3$) and $CeFeO_3$ are the most significant minor components, whereas $SrTiO_3$ and $Th_{0.5}TiO_3$ are generally present in concentrations below 1 mol.%. Unusually high levels of $CeFeO_3$ (up to 11 mol.%) at very low $Na_{0.5}Ce_{0.5}TiO_3$ contents are found in perovskite from Lac de Gras. This perovskite is also enriched in the Nb-bearing components (lueshite and latrappite). A more detailed account of the compositionally "anomalous" perovskite from the Lac de Gras kimberlites is being prepared by the authors of the present study.

The data available in the literature show that loparite, lueshite and tausonite are the most important components in perovskite-group minerals from alkaline rocks (Mitchell & Chakhmouradian 1996, 1999, Chakhmouradian & Mitchell 1997, 1998). The component $CeFeO_3$

TABLE 5. REPRESENTATIVE COMPOSITIONS OF PEROVSKITE FROM KIMBERLITES. NORTH AMERICAN OCCURRENCES

Wt.%	1	2	3	4	5	6	7	8	9	10
Na_2O	0.48	0.28	1.07	0.32	0.53	0.62	0.46	0.62	0.46	0.28
CaO	34.57	31.52	30.27	37.43	36.35	38.28	40.43	37.35	37.02	38.25
SrO	0.26	0.56	0.63	0.24	0.30	0.12	0.23	0.26	0.26	0.35
La_2O_3	1.84	3.21	2.15	0.61	0.74	0.84	n.d	1.39	0.94	0.79
Ce_2O_3	4.84	6.40	6.14	1.94	2.77	2.61	1.02	2.29	2.85	1.49
Pr_2O_3	0.28	0.28	0.35	n.d	0.27	n.d	n.d	n.d	n.d	n.d
Nd_2O_3	0.99	1.22	1.94	0.48	0.59	0.25	n.d	0.31	0.46	0.22
ThO_2	0.46	0.19	2.93	0.52	0.70	0.40	n.d	0.33	0.83	n.d
TiO_2	49.21	38.05	43.78	54.27	54.53	55.88	55.81	54.57	54.37	55.30
SiO_2	n.d	0.19	0.08	n.d	n.d	0.24	0.22	0.28	n.d	n.d
ZrO_2	n.d	2.44	0.47	n.d	n.d	n.d	n.d	n.d	n.d	n.d
Al_2O_3	0.60	0.66	0.35	0.27	0.17	0.32	0.48	0.40	n.d	n.d
Fe_2O_3*	4.18	5.65	5.24	1.28	1.24	1.29	1.96	1.27	1.15	1.14
Nb_2O_5	1.67	8.55	3.65	0.86	0.84	0.89	0.93	0.86	0.70	0.72
Ta_2O_5	0.50	0.39	1.05	0.35	0.24	n.d	0.03	n.d	0.36	0.29
Total	99.88	99.59	100.10	98.57	99.27	101.74	101.57	99.93	99.40	98.83
Structural formulae based on 3 atoms of oxygen										
Na	0.022	0.014	0.052	0.015	0.024	0.027	0.020	0.028	0.021	0.013
Ca	0.894	0.859	0.819	0.946	0.919	0.936	0.977	0.932	0.936	0.958
Sr	0.004	0.008	0.009	0.003	0.004	0.002	0.003	0.004	0.004	0.005
La	0.016	0.030	0.020	0.005	0.006	0.007	-	0.012	0.008	0.007
Ce	0.043	0.060	0.057	0.017	0.024	0.022	0.008	0.020	0.025	0.013
Pr	0.002	0.003	0.003	-	0.002	-	-	-	-	-
Nd	0.009	0.011	0.018	0.004	0.005	0.002	-	0.003	0.004	0.002
Th	0.003	0.001	0.017	0.003	0.004	0.002	-	0.002	0.004	-
$\sum A$	0.993	0.986	0.995	0.993	0.988	0.998	1.008	1.001	1.002	0.998
Ti	0.894	0.727	0.831	0.962	0.967	0.959	0.947	0.955	0.966	0.972
Si	-	0.005	0.002	-	-	0.005	0.005	0.007	-	-
Zr	-	0.030	0.006	-	-	-	-	-	-	-
Al	0.017	0.020	0.010	0.008	0.005	0.009	0.013	0.011	-	-
Fe	0.076	0.108	0.100	0.023	0.022	0.022	0.033	0.022	0.020	0.020
Nb	0.018	0.098	0.042	0.009	0.009	0.009	0.009	0.009	0.007	0.007
Ta	0.003	0.003	0.007	0.002	0.002	-	-	-	0.002	0.002
$\sum B$	1.008	0.991	0.998	1.004	1.005	1.004	1.007	1.004	0.995	1.001
Mol.% end-members										
$NaNbO_3$	2.16	1.41	4.84	1.15	1.06	0.92	0.96	0.91	0.97	0.95
Loparite	-	-	0.59	0.65	2.77	3.65	2.07	3.78	2.24	0.65
$CeFeO_3$	7.05	10.53	9.39	2.30	2.41	1.27	-	1.51	2.53	1.82
$CaTiO_3$	89.91	79.15	80.35	95.01	92.59	93.58	96.67	93.10	93.02	96.10
$CaZrO_3$	-	3.04	0.59	-	-	-	-	-	-	-
$SrTiO_3$	0.37	0.81	0.88	0.33	0.41	0.16	0.30	0.35	0.35	0.48
$Th_{0.5}TiO_3$	0.51	0.20	3.36	0.56	0.76	0.42	-	0.35	0.89	-
Latrappite	-	4.86	-	-	-	-	-	-	-	-

1-3 discrete grains from different intrusions, Lac de Gras (NWT, Canada); 4-10 Somerset Island (Nunavut Territory, Canada): 4-5 unzoned discrete crystals (Nikos), 6-7 core and rim of a weakly zoned crystal, respectively (Elwin Bay), 8 unzoned crystal (Elwin Bay), 9-10 core and rim of a weakly zoned crystal, respectively (Tunraq). * Total Fe as Fe_2O_3; n.d = not detected. Loparite = $Na_{0.5}Ce_{0.5}TiO_3$; latrappite = $CaFe_{0.5}Nb_{0.5}O_3$.

is insignificant in these minerals, and elevated Fe contents in perovskite from some carbonatites can be assigned entirely to the latrappite end-member ($CaFe_{0.5}Nb_{0.5}O_3$) (Chakhmouradian & Mitchell 1997, Mitchell *et al.* 1998). Hence, for comparative purposes, we plotted the compositions obtained in the present study in terms of the end-members perovskite – loparite – lueshite (Figs. 5–8). From these diagrams, it is obvious that perovskite from kimberlites exhibits a very limited variation in composition, and, in most occurrences, the composition points cluster parallel to the join perovskite–loparite. In some kimberlites, the normal pattern of zonation is expressed as a decreasing content of loparite toward the rim (*e.g.*, Fig. 5: Matsoku, Wesselton and Frank Smith). In other cases, the normal pattern of zonation is less conspicuous, as it involves a decrease in $CeFeO_3$, rather than the loparite component (Fig. 6: Xi-Yu, China). Note also that the oscillatory zonation observed in perovskite from Benfontein cannot be described by a single evolutionary trend in the terms of the end-members perovskite – loparite – lueshite (Fig. 5).

In the majority of kimberlites, reaction-induced rims of perovskite are very similar to discrete crystals in terms of their composition (Figs. 5, 7 and 8). Subtle compositional differences observed in some intrusions invariably arise from lower *REE* and Nb contents in the reaction-induced rims (Table 1, anal. 9–10, Fig. 5).

TABLE 6. REPRESENTATIVE COMPOSITIONS OF PEROVSKITE FROM KIMBERLITES. NORTH AMERICAN OCCURRENCES

Wt.%	1	2	3	4	5	6	7	8
Na_2O	0.28	0.69	0.25	0.95	1.60	0.89	1.15	0.93
CaO	37.16	36.99	37.32	36.24	31.46	37.03	35.77	34.34
SrO	0.30	0.44	0.38	0.18	0.40	0.24	0.27	0.18
La_2O_3	0.96	1.03	1.38	1.48	1.63	1.16	0.76	1.09
Ce_2O_3	2.62	2.87	2.62	3.40	5.60	2.65	3.50	4.30
Pr_2O_3	0.31	n.d	0.37	0.25	0.30	n.d	0.13	0.35
Nd_2O_3	0.50	0.51	0.74	0.75	1.84	0.31	0.82	1.34
ThO_2	0.52	1.07	0.11	n.d	1.84	n.d	0.61	1.20
TiO_2	54.70	54.54	54.14	53.24	50.81	51.73	53.84	51.95
SiO_2	n.d	n.d	n.d	0.31	0.23	0.27	0.14	0.41
Al_2O_3	0.37	0.33	n.d	0.32	0.19	0.31	0.24	0.34
Fe_2O_3*	1.29	1.44	1.61	1.19	1.43	2.62	0.97	1.21
Nb_2O_5	0.67	0.72	0.82	2.14	2.39	3.51	1.47	1.88
Ta_2O_5	0.25	n.d	0.25	n.d	0.27	n.d	0.22	0.08
Total	99.93	100.63	99.99	100.45	99.99	100.72	99.89	99.60
				Structural formulae based on 3 atoms of oxygen				
Na	0.013	0.031	0.011	0.043	0.076	0.040	0.053	0.043
Ca	0.932	0.925	0.940	0.909	0.821	0.924	0.902	0.881
Sr	0.004	0.006	0.005	0.002	0.006	0.003	0.004	0.002
La	0.008	0.009	0.012	0.013	0.015	0.010	0.007	0.010
Ce	0.022	0.025	0.023	0.029	0.050	0.023	0.030	0.038
Pr	0.003	-	0.003	0.002	0.003	-	0.001	0.003
Nd	0.004	0.004	0.006	0.006	0.016	0.003	0.007	0.011
Th	0.003	0.006	0.001	-	0.010	-	0.003	0.007
$\sum A$	0.989	1.006	1.001	1.004	0.997	1.003	1.007	0.995
Ti	0.962	0.957	0.957	0.938	0.931	0.906	0.954	0.935
Si	-	-	-	0.007	0.006	0.006	0.003	0.010
Al	0.010	0.009	-	0.009	0.005	0.009	0.007	0.010
Fe	0.023	0.025	0.028	0.021	0.026	0.046	0.017	0.022
Nb	0.007	0.008	0.009	0.023	0.026	0.037	0.016	0.020
Ta	0.002	-	0.002	-	0.002	-	0.001	0.001
$\sum B$	1.004	0.999	0.996	0.998	0.996	1.004	0.998	0.998
				Mol.% end-members				
$NaNbO_3$	0.88	0.75	1.03	2.25	1.69	2.08	2.79	3.69
Loparite	0.81	4.67	0.22	4.07	7.02	4.45	9.44	0.64
$CeFeO_3$	3.38	1.39	4.28	2.97	0.93	3.95	3.56	3.18
$CaTiO_3$	93.96	91.48	93.83	90.47	89.35	87.96	81.62	92.17
$SrTiO_3$	0.41	0.59	0.52	0.24	0.36	0.25	0.56	0.32
$Th_{0.5}TiO_3$	0.56	1.12	0.12	-	0.65	1.31	2.03	-

1-3 Peuyuk, Somerset Island (Nunavut Territory, Canada): 1 unzoned discrete crystal (intrusion B), 2-3 unzoned discrete crystals (intrusion C); 4-8 Kirkland Lake (Ontario, Canada): 4 reaction-induced rim on magnesian ilmenite, 5-6 core and rim of a zoned crystal, 7-8 glomerocryst with complex oscillatory-type zoning. * Total Fe as Fe_2O_3; n.d = not detected. Loparite = $Na_{0.5}Ce_{0.5}TiO_3$.

DISCUSSION AND CONCLUSIONS

The data obtained in the present study confirm that in most kimberlites, discrete crystals are the typical mode of perovskite occurrence. These may or may not be accompanied by a reaction-induced rim of perovskite on ilmenite and other macrocrystic phases. Perovskite clearly postdates minerals of the macrocryst suite, and crystallizes nearly simultaneously with groundmass spinel belonging to the magnesian ulvöspinel – magnetite or spinel–hercynite series. Crystallization of perovskite typically ceases prior to resorption and development of an atoll rim on these spinels. In common with the spinel, perovskite may become unstable during the final evolutionary stages, and reacts with a CO_2-rich fluid precipitating calcite and serpentine (Mitchell & Chakhmouradian 1998a). Typical patterns of alteration observed in perovskite in kimberlite result from the combined effects of resorption, cation leaching and replacement by late-stage minerals, most commonly one or more TiO_2 polymorphs and ilmenite. Banfield & Veblen (1992) have shown that conversion of perovskite to TiO_2 does not necessarily involve dissolution of the $CaTiO_3$ host, and may occur *in situ* by re-arrangement of TiO_6 octahedra. Undoubtedly, replacement of

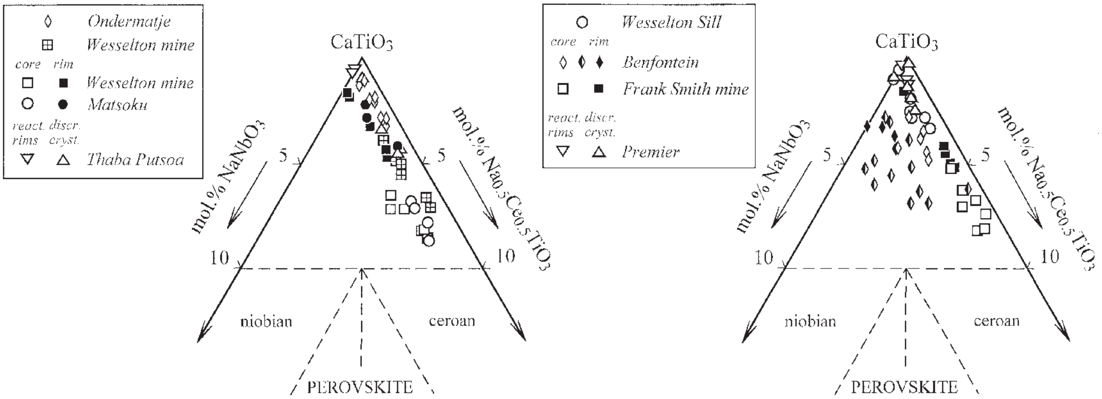

FIG. 5. Composition (mol.%) of perovskite from some kimberlite occurrences in Africa.

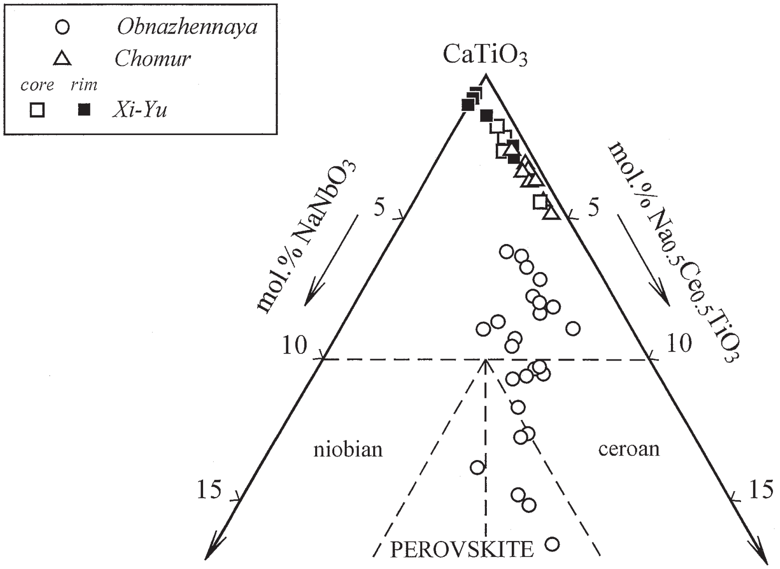

FIG. 6. Composition (mol.%) of perovskite from some kimberlite occurrences in Asia.

perovskite by ilmenite may occur in a similar manner, as $CaTiO_3$ and $FeTiO_3$ have greater structural similarity than any of the naturally occurring TiO_2 polymorphs. Conversion of perovskite to ilmenite would involve tilting of TiO_6 octahedra accompanied by ion exchange at larger cationic sites. Lacking transmission electron microscopy data, it is unclear whether the alteration patterns observed in kimberlites result from *in situ* replacement of perovskite (incongruent dissolution), or from its resorption and the subsequent precipitation of late-stage oxide phases on the $CaTiO_3$ substrate.

Conversion of perovskite to rutile has been assessed thermodynamically by Nesbitt *et al.* (1981). As anatase, and not rutile, is the TiO_2 polymorph present at least in some kimberlites, we estimated the stability limits of both anatase and rutile relative to perovskite [reaction (1) above]. Importantly, both reactions (perovskite ⇔ rutile and perovskite ⇔ anatase) involve a notable change in volume of the solid phases; at elevated pressures and temperatures, this change affects the Gibbs free energy of the reaction. Consequently, this process does not only depend on temperature and $P(CO_2)$, but also on total pressure in the system. The combined phase diagram illustrating relationships between the TiO_2 polymorphs and perovskite is shown in Figure 9. Our results for the reaction perovskite ⇔ rutile at P = 1 MPa

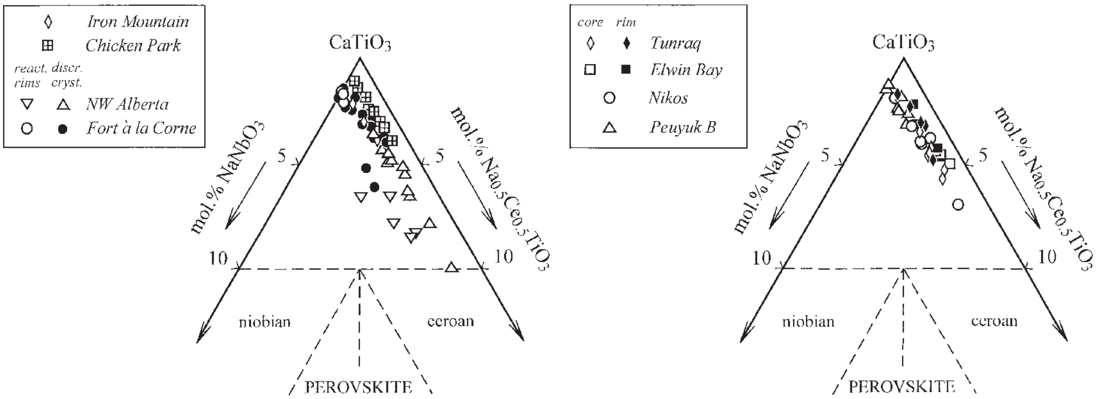

FIG. 7. Composition (mol.%) of perovskite from some kimberlite occurrences in North America.

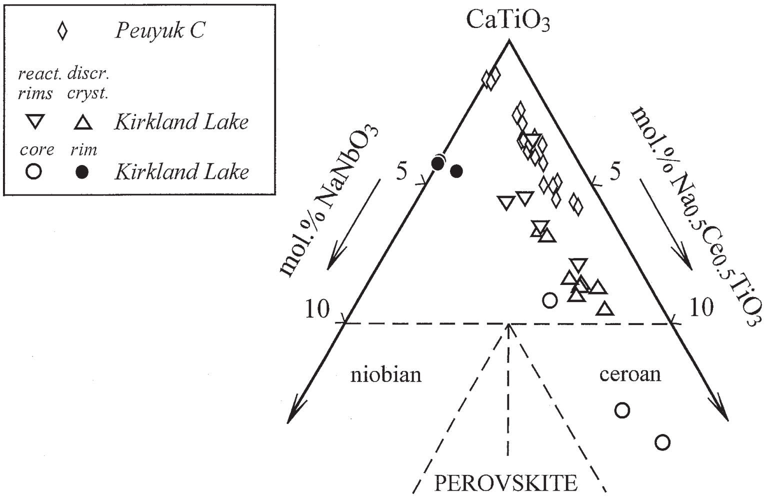

FIG. 8. Composition (mol.%) of perovskite from some kimberlite occurrences in North America.

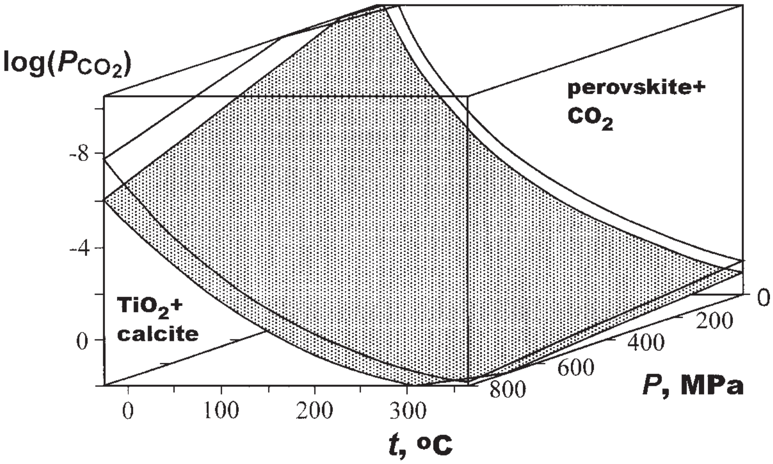

FIG. 9. Equilibrium surfaces corresponding to the reactions of perovskite conversion to anatase (lower, stippled) and rutile (upper, transparent) in terms of total pressure, temperature and $P(CO_2)$ in the system.

are in excellent agreement with the calculations of Nesbitt *et al.* (1981). From this diagram, we can conclude that crystallization of anatase requires somewhat higher $P(CO_2)$ or lower temperatures in comparison with the reaction producing rutile. In the range of reasonable $P(CO_2)$ values, both replacement reactions are confined to relatively low temperatures (<350°C) and pressures (<2 kbar).

The process of perovskite replacement by ilmenite [reaction (3)] is not contingent on pressure, but strongly depends on the activities of individual divalent species (Ca^{2+}, Mg^{2+}, Mn^{2+} and Fe^{2+}) in a fluid. Generally low contents of $MgTiO_3$ in the late-stage ilmenite can be readily explained using Figure 10. Replacement of $CaTiO_3$ by $MgTiO_3$ is virtually independent of temperature and occurs only at relatively high activities of Mg^{2+} in the fluid [$\log a(Ca^{2+})/a(Mg^{2+}) < 1.5$], whereas crystallization of ilmenite requires significantly lower values of $a(Fe^{2+})$. A univariant curve corresponding to the equilibrium between $CaTiO_3$ and $MnTiO_3$ is tempera-

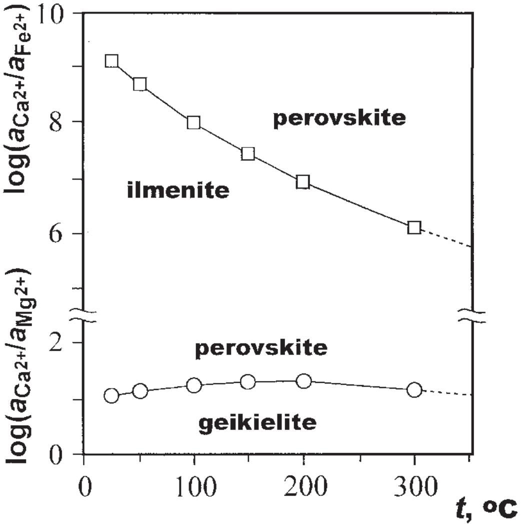

FIG. 10. Isobaric curves (P = 1 MPa) corresponding to the equilibria of perovskite with ilmenite-group minerals.

ture-dependent and plots between the perovskite – geikielite and perovskite – ilmenite curves. Hence, alteration of perovskite will produce $FeTiO_3$-dominant reaction rims with some enrichment in $MnTiO_3$ even at very high concentrations of Mg in the deuteric fluid.

The absence of replacement rims on perovskite from crater-facies kimberlites attests to the significance of kinetic factors in the alteration processes. Nesbitt *et al.* (1981) have demonstrated that the equilibrium concentration of Ca^{2+} in a leachant and, hence, the leach rate vary dramatically with temperature. Furthermore, precipitation of secondary calcite, apatite or Ca-bearing silicates will decrease the actual concentration of Ca^{2+} in the system, shifting the equilibrium toward the end-products in both principal replacement reactions [(1) and (3)], thus increasing the leach rate. In crater-facies kimberlites, crystallization of late-stage Ca minerals is very rapid, confined to vesicles (as in Lac de Gras rocks: Chakhmouradian & Mitchell 2000), and is unlikely to accelerate leaching of Ca^{2+} from perovskite. The kinetics of perovskite dissolution in fluids of different composition and temperature are poorly known, and further experimental work is required.

In terms of composition, perovskite from kimberlites approaches the ideal formula $CaTiO_3$, and normally contains less than 7 mol.% of other end-members, primarily lueshite ($NaNbO_3$), loparite ($Na_{0.5}Ce_{0.5}TiO_3$) and $CeFeO_3$. Evolutionary trends exhibited by perovskite from most localities are relatively insignificant and typically involve some decrease in loparite or $CeFeO_3$ content toward the rim. Oscillatory patterns of zonation are relatively rare and cannot be explained in terms of a simple extrinsic driving mechanism (*sensu* Shore & Fowler 1996), such as convection or cyclic changes in $f(O_2)$. Here, we shall not discuss the key arguments against possible extrinsic mechanisms (*e.g.*, high settling rate of perovskite in a differentiating kimberlitic magma, and the lack of correlation among patterns exhibited by different crystals), as such a discussion is clearly beyond the scope of this work. We suggest that the appearance of oscillatory zonation in some perovskite samples is controlled by intrinsic mechanisms, *i.e.*, fluctuations in the rate of chemical and thermal diffusion in a layer adjacent to the growing crystal. For the more detailed discussions of such mechanisms, the reader is referred to the recent reviews by Shore & Fowler (1996) and Pearce (1994).

Three compositional features of perovskite from kimberlites will be discussed here in more detail: (i) enrichment of some samples in *LREE*, Th and Nb, (ii) negligible Sr contents, and (iii) generally low Fe contents in the majority of samples. The high concentrations of *LREE*, Nb and Th in perovskite do not correlate with a particular kimberlite facies, degree of differentiation of the host rock, or mineral paragenesis. In addition, similar levels of "incompatible" elements can be found in samples from highly contaminated and fresh kimberlites (*cf.* data for Fort à la Corne and Kirkland Lake in Tables 4 and 6). Hence, we suggest here that the high contents of *LREE*, Th and Nb in perovskite result from inherent enrichment of some kimberlitic magmas in these elements. The source of such enrichment is debatable, primarily because the source of kimberlitic magma *sese* remains poorly understood (for discussion, see Mitchell 1995, p. 366–372). Processes of metasomatism in the upper mantle have been envisioned as a potential mechanism of enhancement, whereas subsequent sequestration of "incompatible" elements in kimberlitic magma is achieved through small-scale partial melting (Mitchell 1986, 1995). As the mineral constitution of the upper-mantle source will vary with depth, and the depth of magma generation is unknown, any attempt to relate the *LREE*-, Nb- and Th-enrichment of perovskite in some kimberlites to a particular geological process would be purely speculative. It is noteworthy, however, that in some occurrences, the syn- and post-emplacement processes such as differentiation (Benfontein) and contamination (Lac de Gras) may have contributed to the accumulation of "incompatible" elements in perovskite.

The low levels of Sr in kimberlitic perovskite are in agreement with the experimental data of Mitchell (1997b), indicating that Sr is preferentially partitioned into carbonates. This conclusion is further supported by the occurrence of Sr-rich (up to 6.5 wt.% SrO) perovskite in lamproites devoid of primary carbonate phases (Mitchell & Chakhmouradian 1999). In addition to calcite, apatite-group minerals may serve as a primary repository for Sr in kimberlites (Chakhmouradian & Mitchell 2000). In the absence of melilite, Sr is partitioned strongly into apatite relative to perovskite (Rass & Laputina 1996).

With a few exceptions, perovskite from kimberlites is poor in Fe (<2.3 wt.% Fe_2O_3). As Fe is incorporated in naturally occurring perovskite only in the trivalent form (Mitchell *et al.* 1998, Muir *et al.* 1984), the paucity of Fe in perovskite indicates low $f(O_2)$ during the precipitation of groundmass minerals ($10^{-19} – 10^{-22}$ bar: Mitchell 1986). This conclusion is consistent with the compositional trend of decreasing Fe^{3+} content in ilmenite-group minerals from kimberlites (*e.g.*, Chakhmouradian & Mitchell 1999). Elevated Fe contents found in some perovskite samples probably result from contamination of the kimberlitic magma with relatively oxidized crustal material. One such an example may be the Fe–Al-rich perovskite from the Lac de Gras area (up to 8.3 wt.% Fe_2O_3 and 1.5 wt.% Al_2O_3).

In conclusion, we point out that the above generalizations should be treated with caution. For example, perovskite may potentially crystallize before primary carbonates and act as a sink for Sr, compositionally approaching its counterparts in olivine lamproites (Mitchell & Chakhmouradian 1999). Another example is the absence of a TiO_2 rim on perovskite crystals in many kimberlites. This absence does not necessarily indicate low $P(CO_2)$ in the system because, at high $a(Ca^{2+})$, the leaching of Ca from perovskite is effectively buffered by crystallization of calcite. Therefore, the mode of occurrence of perovskite and its compositional variation can be interpreted only in the context of other available geological and mineralogical data.

Acknowledgements

This study is supported by the Natural Sciences and Engineering Research Council of Canada. We gratefully acknowledge the help of Ann Hammond and Allan MacKenzie with sample preparation and analytical work, respectively. Drs. M.G. Kopylova and W.L. Griffin provided several constructive comments on the early version of the manuscript. We are indebted to the editor, Dr. Robert F. Martin, for his continual editorial attention. We also thank Dr. Bruce Kjarsgaard (Geological Survey of Canada) and Kennecott Canada Exploration Inc. for providing some of the samples used in the present study.

References

Banfield, J.F. & Veblen, D.R. (1992): Conversion of perovskite to anatase and TiO_2 (B): a TEM study and the use of fundamental building blocks for understanding relationships among the TiO_2 minerals. *Am. Mineral.* **77**, 545-557.

Blagul'kina, V.A. & Tarnovskaya, A.N. (1975): On perovskite from kimberlites of Yakutia. *Zap. Vses. Mineral. Obshchest.* **104**, 703-710 (in Russ.).

Boctor, N.Z. & Boyd, F.R. (1980): Oxide minerals in the Liqhobong kimberlite, Lesotho. *Am. Mineral.* **65**, 631-638.

________ & ________ (1981): Oxide minerals in a layered kimberlite–carbonatite sill from Benfontein, South Africa. *Contrib. Mineral. Petrol.* **76**, 253-259.

_______ & Meyer, H.O.A. (1979): Oxide and sulphide minerals in kimberlite from Green Mountain, Colorado. *In* Kimberlites, Diatremes and Diamonds: their Geology, Petrology and Geochemistry. Proc. 2nd Int. Kimberlite Conf., Vol. 1 (F.R. Boyd & H.O.A. Meyer, eds.). Am. Geophys. Union, Washington, D.C. (217-228).

Chakhmouradian, A.R. & Mitchell, R.H. (1997): Compositional variation of perovskite-group minerals from the carbonatite complexes of the Kola Alkaline Province, Russia. *Can. Mineral.* **35**, 1293-1310.

________ & ________ (1998): Compositional variation of perovskite-group minerals from the Khibina Complex, Kola Peninsula, Russia. *Can. Mineral.* **36**, 953-970.

________ & ________ (1999): Niobian ilmenite, hydroxylapatite and sulfatian monazite: alternative hosts for incompatible elements in calcite kimberlite from Internatsional'naya, Yakutia. *Can. Mineral.* **37**, 1177-1189.

________ & ________ (2000): Unusual accessory minerals in kimberlites of the Lac de Gras area (NWT, Canada): insight into the evolutionary history of the host rocks. *Geol. Assoc. Can. – Mineral. Assoc. Can., Program Abstr.* **25**, *file* 375.pdf.

Dawson, J.B. & Hawthorne, J.B. (1973): Magmatic sedimentation and carbonatitic differentiation in kimberlite sills at Benfontein, South Africa. *J. Geol. Soc. London* **129**, 61-85.

Grunin, V.S., Razumenko, M.V., Patrina, I.V., Filatov, S.K. & Alekseyeva, T.V. (1983): Mode of existence and abundance of TiO_2 – rutile, anatase and brookite. *Dokl. Acad. Sci. USSR, Earth Sci. Sect.* **268**, 149-150.

Haggerty, S.E. (1987): Metasomatic mineral titanates in upper mantle xenoliths. *In* Mantle Xenoliths (P.H. Nixon, ed.). John Wiley & Sons, New York, N.Y. (671-690).

Kapustin, Yu.L. (1964): Accessory rare-metal mineralogy of carbonatites at Kola Peninsula. *In* Mineralogy and Genetic Features of Alkaline Complexes. Nauka Press, Moscow, Russia (in Russ., 135-194).

Kimura, S. & Muan, A. (1971): Phase relations in the system CaO – iron oxide – titanium oxide under strongly reducing conditions. *Am. Mineral.* **56**, 1347-1358.

Kopylova, M.G., Gurney, J.J. & Daniels, L.R.M. (1997a): Mineral inclusions in diamonds from the River Ranch kimberlite, Zimbabwe. *Contrib. Mineral. Petrol.* **129**, 366-384.

________, Rickard, R.S., Kleyenstueber, A., Taylor, W.R., Gurney, J.J. & Daniels, L.R.M. (1997b): First occurrence of strontian K–Cr loparite and Cr-chevkinite in diamonds. *Russ. Geol. Geophys.* **38**, 405-420.

MITCHELL, R.H. (1984): Mineralogy and origin of carbonate-rich segregations in a composite kimberlite sill. *Neues Jahrb. Mineral., Abh.* **150**, 185-197.

________ (1986): *Kimberlites: Mineralogy, Geochemistry, and Petrology*. Plenum Press, New York, N.Y.

________ (1995): *Kimberlites, Orangeites, and Related Rocks*. Plenum Press, New York, N.Y.

________ (1996): Perovskites: a revised classification scheme for an important rare earth element host in alkaline rocks. *In* Rare Earth Minerals: Chemistry, Origin and Ore Deposits (A.P. Jones, F. Wall & C.T. Williams, eds.). *Mineral. Soc.* (*UK*) *Ser.* **7**, Chapman & Hall, London, U.K. (41-76).

________ (1997a): *Kimberlites, Orangeites, Lamproites, Melilitites, and Minettes: a Petrographic Atlas*. Almaz Press, Thunder Bay, Ontario.

________ (1997b): Preliminary studies of the solubility and stability of perovskite group compounds in the synthetic carbonatite system calcite–portlandite. *J. Afr. Earth Sci.* **25**, 147-158.

________ & CHAKHMOURADIAN, A.R. (1996): Compositional variation of loparite from the Lovozero alkaline complex, Russia. *Can. Mineral.* **34**, 977-90.

________ & ________ (1998a): Instability of perovskite in a CO_2-rich environment: examples from carbonatite and kimberlite. *Can. Mineral.* **36**, 939-952.

________ & ________ (1998b): Th-rich loparite from the Khibina alkaline complex, Kola Peninsula: isomorphism and paragenesis. *Mineral. Mag.* **62**, 341-353.

________ & ________ (1999): Sr-bearing perovskite and loparite from lamproite and agpaitic nepheline syenite pegmatites. *Can. Mineral.* **37**, 99-112.

________, CHOI, JIN-BEOM, HAWTHORNE, F.C., MCCAMMON, C.A. & BURNS, P.C. (1998): Latrappite: a re-investigation. *Can. Mineral.* **36**, 107-116.

________ & CLARKE, D.B. (1976): Oxide and sulphide mineralogy of the Peyuk kimberlite, Somerset Island, N.W.T., Canada. *Contrib. Mineral. Petrol.* **56**, 157-172.

MUIR, I.J., METSON, J.B. & BANCROFT, G.M. (1984): ^{57}Fe Mössbauer spectra of perovskite and titanite. *Can. Mineral.* **22**, 689-694.

NESBITT, H.W., BANCROFT, M.G., FYFE, W.S., KARKHANIS, S.N., NISHIJIMA, A. & SHIN, S. (1981): Thermodynamic stability and kinetics of perovskite dissolution. *Nature* **289**, 358-362.

PASTERIS, J.D. (1983): Spinel zonation in the De Beers kimberlite, South Africa: possible role of phlogopite. *Can. Mineral.* **21**, 41-58.

PEARCE, T.H. (1994): Recent work on oscillatory zoning in plagioclase. *In* Feldspars and Their Reactions. (I. Parsons, ed.). NATO Adv. Study Inst., Kluwer Acad. Publ., Dordrecht, The Netherlands (313-349).

RASS, I.T. & LAPUTINA, I.P. (1996): Composition and zonation of accessory minerals in alkali ultrabasites as indicators of the composition and differentiation of the primary magmas. *Geochem. Int.* **33**(2), 62-77.

SHORE, M. & FOWLER, A.D. (1996): Oscillatory zoning in minerals: a common phenomenon. *Can. Mineral.* **34**, 1111-1126.

SMIRNOV, G.I. (1959): On the mineralogy of Siberian kimberlites. *Trudy Yakut. Fil., Akad. Nauk SSSR* (*Proc. Yakut. Branch Acad. Sci. USSR*), *Ser. Geol.* **4**, 47-73 (in Russ.).

VISHNEVSKII, A.A., KOLESNIK, YU.N. & KHAR'KIV, A.D. (1984): On the genesis of kelyphytic rims on pyrope from kimberlites. *Mineral. Zh.* **6**(4), 55-66 (in Russ.).

Received December 3, 1999, revised manuscript accepted May 6, 2000.